Oxytocin facilitates social behavior of female rats via selective modulation of interneurons in the medial prefrontal cortex

Stephanie Schimmer[1,2,*], Arthur Lefevre[1,2,*], Julia Lebedeva[1,2], Andrey Rozov[3,4,5], Alan Kania[1,2], Androniki Raftogianni[1,2,6], Konstantinos Afordakos[1,2], Rishika Tiwari[7], Shai Netser[7], Ryan Patwell[1,2], Dimitri Hefter[8], Arjen Boender[9], Yuval Podpecan[10], Tim Schubert[10], Anna Sanetra[11], Aleksandra Trenk[11], Anna Gugula[11], Rene Hurlemann[12], Ferdinand Althammer[10], Anna Blasiak[11], Sarah Melzer[13], Hannah Monyer[14], Shlomo Wagner[7], Marina Eliava[1,2,#], Valery Grinevich[1,2,#]

[1] Department of Neuropeptide Research in Psychiatry, Central Institute of Mental Health, Medical Faculty Mannheim, University of Heidelberg, Germany
[2] German Center for Mental Health (DZPG), Mannheim-Heidelberg-Ulm, Germany
[3] Institute of Physiology and Pathophysiology, University of Heidelberg, Heidelberg, Germany
[4] Laboratory of Neurobiology, Kazan Federal University, Kazan, Russia
[5] Federal Center of Brain Research and Neurotechnologies, Moscow, Russia
[6] Department of Psychology, Laboratory of Behavioral Neuroscience, Faculty of Social Sciences, University of Crete, Greece
[7] Sagol Department of Neurobiology, the Integrated Brain and Behavior Research Center (IBBRC), University of Haifa, Haifa, Israel
[8] Department of Animal Models in Psychiatry, Central Institute of Mental Health, Clinic Psychiatry and Psychotherapy, Mannheim, Germany
[9] Center for Translational Social Neuroscience, Division of Behavioral Neuroscience and Psychiatric Disorders, Emory National Primate Research Center, Emory University, Atlanta, GA, USA.
[10] Institute of Human Genetics, University Hospital Heidelberg, Heidelberg, Germany
[11] Department of Neurophysiology and Chronobiology, Institute of Zoology and Biomedical Research, Jagiellonian University in Krakow, Krakow, Poland
[12] Department of Psychiatry, School of Medicine & Health Sciences, Carl von Ossietzky University of Oldenburg, Oldenburg, Germany
[13] Department of Division of Neuronal Cell Biology (Center for Brain Research), Medical University of Vienna, Vienna, Austria
[14] Department of Clinical Neurobiology, Medical Faculty of Heidelberg University and DKFZ, Heidelberg, Germany

* These authors contributed equally

[#] Corresponding authors:

Marina Eliava, PhD
Department of Neuropeptide Research in Psychiatry
Central Institute of Mental Health
Heidelberg University
J 5 · 68159 Mannheim, Germany
E-mail: marina.eliava@zi-mannheim.de

Valery Grinevich, MD, PhD
Department of Neuropeptide Research in Psychiatry
Central Institute of Mental Health
Heidelberg University
J 5 · 68159 Mannheim, Germany
E-mail: valery.grinevich@zi-mannheim.de

ABSTRACT

The hypothalamic neuropeptide oxytocin is best known for its prosocial behavioral effects. However, the precise anatomical and cellular targets for oxytocin in the cortex during social behavior remain elusive. Here we show that oxytocin neurons project directly to the medial prefrontal cortex where evoked axonal oxytocin release facilitates social behaviors in adult female rats. In conjunction, we report that local oxytocin receptor (OTR^+) expressing cells are predominantly interneurons whose activation promotes social interaction. In particular, in a state of food deprivation, this inhibitory neuronal subpopulation shifts the preference from appetitive food stimuli towards a social stimulus. We further demonstrate that activation of these OTR^+ interneurons inhibits principal cells specifically projecting to the basolateral amygdala, thus providing a putative mechanism of selective oxytocin action in this sociability promoting cortical network.

INTRODUCTION

The neuropeptide oxytocin (OT) plays a central role in modulating various types of social behavior and is primarily synthesized in the hypothalamic paraventricular (PVN), supraoptic (SON), and accessory nuclei (Swanson and Sawchenko 1983, Grinevich, Knobloch-Bollmann et al. 2016). Hypothalamic OT is subsequently transported to the posterior lobe of the pituitary gland and released into the blood where it elicits milk ejection during lactation and uterine contractions during childbirth (Russell, Leng and Douglas 2003). Beyond its peripheral effects, OT is actively involved in modulating neural circuits within the brain. Particularly, direct social interaction strongly activates the OT system via OT neurons in the PVN (Tang, Benusiglio et al. 2020). Axonal collaterals of OT neurons extend to various forebrain regions (Knobloch, Charlet et al. 2012), which coincides with the expression of OT receptors (OTRs) at the site of putative neuropeptide release (Chini, Verhage and Grinevich 2017). These areas, including the central nucleus of the amygdala, nucleus accumbens, ventromedial hypothalamic nucleus, lateral septum, and hippocampus (Marlin and Froemke 2016, Grinevich and Stoop 2018), are pivotal in processing social information, emotional responses, and stress regulation (Veenema and Neumann 2008). The infusion of OT, evoked OT release, or activation of OTR neurons in these regions trigger a broad spectrum of region-specific social behaviors, such as social fear (Knobloch, Charlet et al. 2012, Neumann and Slattery 2015, Menon, Grund et al. 2018), social transmission and contingency (Ferretti, Maltese et al. 2019), social memory (Gur, Tendler and Wagner 2014), social avoidance (Osakada, Yan et al. 2024), and aggression (Calcagnoli, Stubbendorff et al. 2014). With the exception of the auditory cortex in nursing mice, which has been extensively studied by Froemke and colleagues (Marlin, Mitre et al. 2015, Valtcheva and Froemke 2018, Schiavo, Valtcheva et al. 2020), the vast majority of studies demonstrate that the behavioral OT effects are mediated via subcortical brain regions, whereas OT signaling in the cortex is much less explored.

The prefrontal cortex (PFC) is instrumental in orchestrating various higher order and computational aspects of social behavior in mammals, including but not limited to social motivation (Lee, Rhim et al. 2016), recognition of social cues (Gifford III, MacLean et al. 2005, Levy, Tamir et al. 2019), and decision-making (Kingsbury, Huang et al. 2019). The connections of the PFC to other brain areas like the amygdala (Myers-Schulz and Koenigs 2012) and hypothalamus (Reppucci and Petrovich 2016) suggest its role in top-down executive control, such as guiding goal-directed social behaviors. In rodents, the PFC can be divided into three distinct brain subregions, each with unique functions and connectivity: the infralimbic cortex (ILC), the prelimbic cortex (PrL) and the cingulate cortex (Cgt) (Heidbreder and Groenewegen 2003). Considering the widespread influence of OT across various brain regions and a previous study describing the effects of OT in the auditory cortex (Marlin, Mitre et al. 2015) , a modulating role of the neuropeptide in relation to the known functions of the PFC is likely. The involvement of the PFC in attention and internal state control, as evidenced by its engagement in various brain circuits, highlights its importance in processing and responding to environmental stimuli, which could be influenced by OT signaling pathways.

Despite the inspiring demonstrations that OT action and/or OTR-expressing neurons (OTR^+ neurons) in the PFC modulate paternal (He, Young et al. 2019) and sexual behavior (Nakajima, Görlich and Heintz 2014) in voles and mice, respectively, it remains unknown how OT signaling in the PFC affects basic social behavior. To address this question, we aimed to describe the pattern of OT innervation in

the PFC (1), the composition of the local OT receptive cells (2), and their downstream target structures (3), which might promote social behavior in adult female rats.

RESULTS

Evoked OT release in the infralimbic cortex facilitates social behavior in female rats

Both immunohistochemistry (IHC) and viral-based tracing of labeled OT axons from the PVN and SON revealed the presence of OT projections through the entire medial PFC (mPFC) **(Figure 1 A, B1-2)**. The highest density of OT axonal innervation was found in the infralimbic cortex (ILC) compared to the cingulate (Cgt) and prelimbic (PrL) cortices (35.8±7.5 vs. 6.2±3.5 axonal segments per 50µm coronal slice, p<0.0001 unpaired t-test, these and all following results are provided as mean±sd) **(Figure 1 B3)**. Based on this finding, we focused specifically on the ILC area of the mPFC in all follow-up experiments.

Figure 1

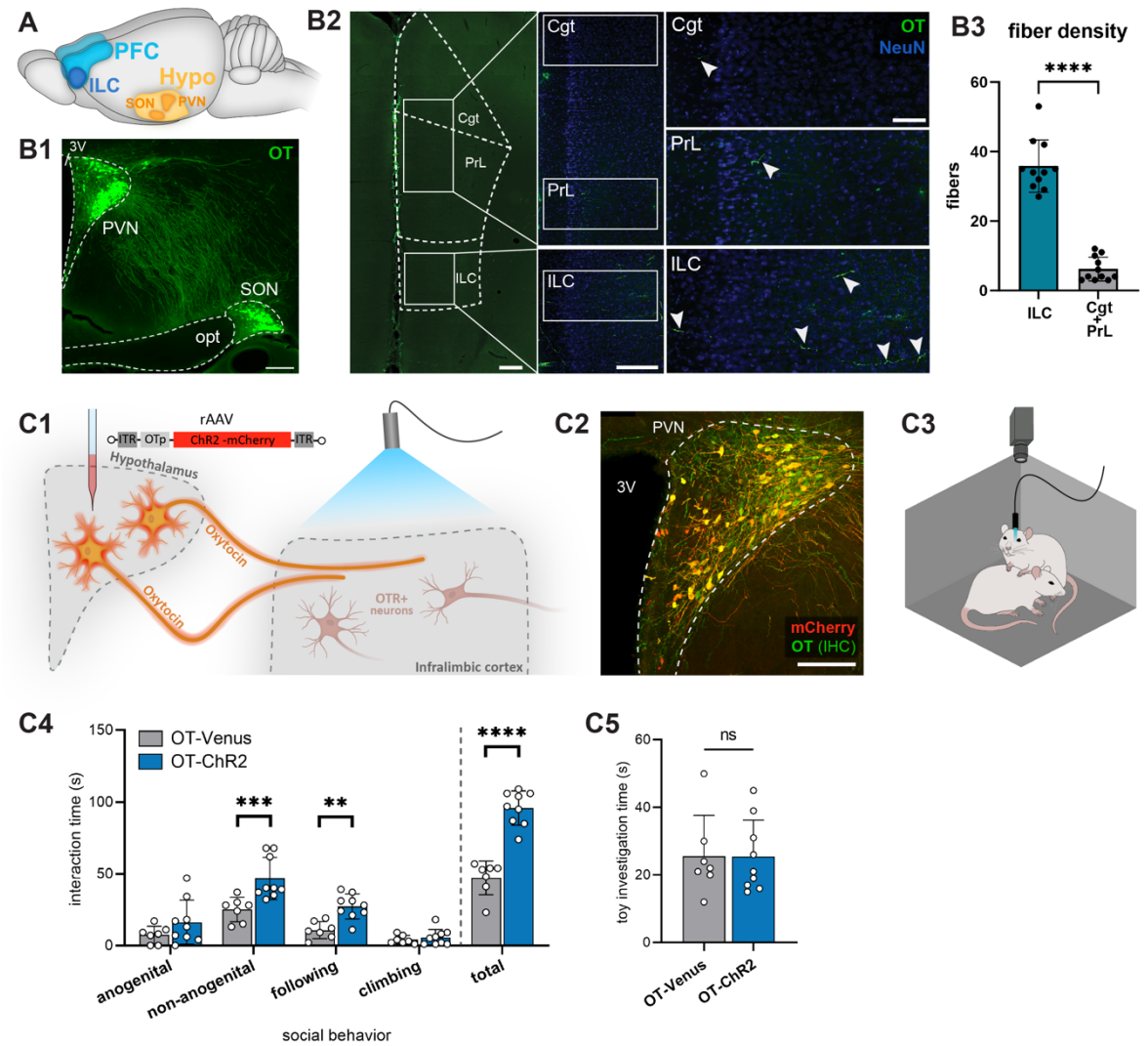

Figure 1 Evoked OT release in the ILC facilitates social behavior in female rats.
A The rat brain regions of interest: PVN and SON in the hypothalamus and the ILC as part of the PFC. **B** OT innervation in the medial prefrontal cortex. **B1** Immunohistochemical staining for OT in the hypothalamus showing OTergic nuclei, the PVN and SON. 3V: third ventricle, opt: optic tract. Scalebar 500µm. **B2** Coronal section of the PFC subdivisions (Cgt, PrL, ILC) and high-magnification images of OT fiber distribution for each sub region: the number of OT fibers (white arrows) is significantly higher in the ILC, compared to Cgt and PrL. Scalebar left: 500µm, middle: 300µm, right 100µm. **B3** Density of OT-positive fibers quantified in digitized images. The number of OT-positive fibers was significantly higher in the ILC, compared to the PFC dorsal subdivisions (n=20 sections obtained from 5 rats).
C Optogenetic activation of OT axons in the ILC during free social interaction. **C1** Injection of a rAAV expressing the excitatory ChR2 under the control of the OT promoter into the hypothalamic nuclei of female rats and implantation of an optic fiber above the ILC. **C2** Injection site showing high specificity of the rAAV-OTp-ChR2-mCherry (red) after counterstaining for OT (green). Scalebar 200µm. **C3** 5-minute social interaction paradigm with an unknown conspecific; blue light (BL) stimulation present for the first two minutes of the session. **C4** Animals injected with OTp-ChR2 (n=9 animals) show significantly increased social interaction

time compared to control animals (injected with OTp-Venus, n=7 animals), especially increased non-anogenital sniffing and following behavior. **C5** Investigation time of a toy rat in the open field remains unaltered by optogenetic activation.

To functionally probe the hypothalamic-ILC pathway, we next expressed channelrhodopsin 2 (ChR2) in OT neurons of the PVN and SON via a recombinant adeno-associated virus (rAAV) equipped with the OT promoter (rAAV-OTp-ChR2-mCherry) and implanted an optic fiber above the ILC **(Figure 1 C1-2)**. Utilizing this approach, we could previously establish that blue light (BL) stimulation leads to an evoked OT release in the target region (Knobloch, Charlet et al. 2012). After 3 weeks of viral expression, the social behavior of female rats was analyzed in an open field (OF) arena where they were exposed to an unknown, age-, strain- and sex-matched conspecific **(Figure 1 C3)**. In keeping with previous studies (Knobloch, Charlet et al. 2012, Tang, Benusiglio et al. 2020), we employed adult female rats to exclude the aggressive component of social behavior often observed between unfamiliar males (Schuster, Berger and Swanson 1988). Social behaviors were significantly increased (total interaction time 47.1±11.8s vs 95.9±11.9s, $p<0.0001$ two-way ANOVA) during and immediately after optogenetic stimulation (120 sec, 30 Hz,10 ms pulses, laser power ~10 mW) compared to the control group expressing Venus fluorescent protein instead of ChR2. This effect was significantly facilitated by increased non-anogenital sniffing and following behaviors (25.0±8.5s vs 46.8±14.7s, $p=0.0002$ and 10.7±5.9s vs 27.2±8.6s, $p=0.0059$, respectively, two-way ANOVA with Sidák's multiple comparison) **(Figure 1 C4)**. Importantly, no difference was observed between the two groups when comparing their time spent investigating a toy rat (25.6±12.0s vs 25.4±10.8s, $p=0.98$ unpaired t-test) **(Figure 1 C5)**, confirming the importance of the social factor as the driver of the observed behavior as opposed to general interest and novelty. No changes in locomotory activity, exploratory, or anxiety-related behaviors were found **(Extended Data Figure S1)**. Altogether, these results indicate that optogenetic activation of the OTergic hypothalamic-ILC projections are sufficient to enhance social behavior in female rats.

OTR$^+$ neurons in the ILC are intrinsically active during social behavior

Next, to label and manipulate OTR$^+$ neurons in the ILC we utilized newly generated OTR-Cre knock-in rats (Iwasaki, Lefevre et al. 2023). The rats were injected with an rAAV expressing GFP in a Cre-dependent (double-floxed-inverted-orientation: DIO) manner into the ILC (rAAV-Ef1a-DIO-GFP) **(Figure 2 A1,** see also **Extended Data Figure S2** for further characterization of the rat line and protein expression). Among the entire ILC neuronal population, visualized by NeuN **(Figure 2 A2)**, 9.5% of neurons expressed OTRs with a higher occurrence in superficial layers 2/3 compared to the deeper layers 5/6 (12.7% and 8.9%, respectively) **(Figure 2 A3)**. To monitor OTR$^+$ neuronal intrinsic activity, we performed *in vivo* fiber photometry during social interaction utilizing an rAAV expressing a Cre-dependent Ca^{2+} sensor (rAAV-Efa1-DIO-GCaMP6s) and implanted optic fibers **(Figure 2 B1-2)**. During repeated 5-minute social interaction sessions, multiple behavioral events (non-anogenital and anogenital sniffing, and investigation of a toy) were scored and the aligned calcium activity of OTR$^+$ neurons was compared **(Figure 2 B3)**. Social sniffing behaviors performed by the test rat were accompanied by a significant increase of calcium signal in OTR$^+$ neurons compared to baseline (z score for anogenital: 0.12±0.011, non-anogenital: 0.18±0.008) and compared to toy investigation (0.04±0.013) (these results are provided as mean±sem, $p<0.0001$ for anogenital and non-anogenital sniffing compared to baseline) **(Figure 2 B4)**. Furthermore, we also compared the amplitude of calcium signals during social events that were initiated by the test rat (active social behavior) with the social events performed by the stimulus rat (received social behavior) **(Figure 2 B5)**. We observed that only

active social behavior increased calcium dynamics in OTR⁺ neurons in the ILC (z score for active: 0.12±0.006, p<0.0001, received: -0,01±0.008, p=0.88, results are provided as mean±sem) compared to baseline **(Figure 2 B6)**. Therefore, we conclude that OTR⁺ neurons in the ILC are highly and specifically active during active social behavior.

Figure 2

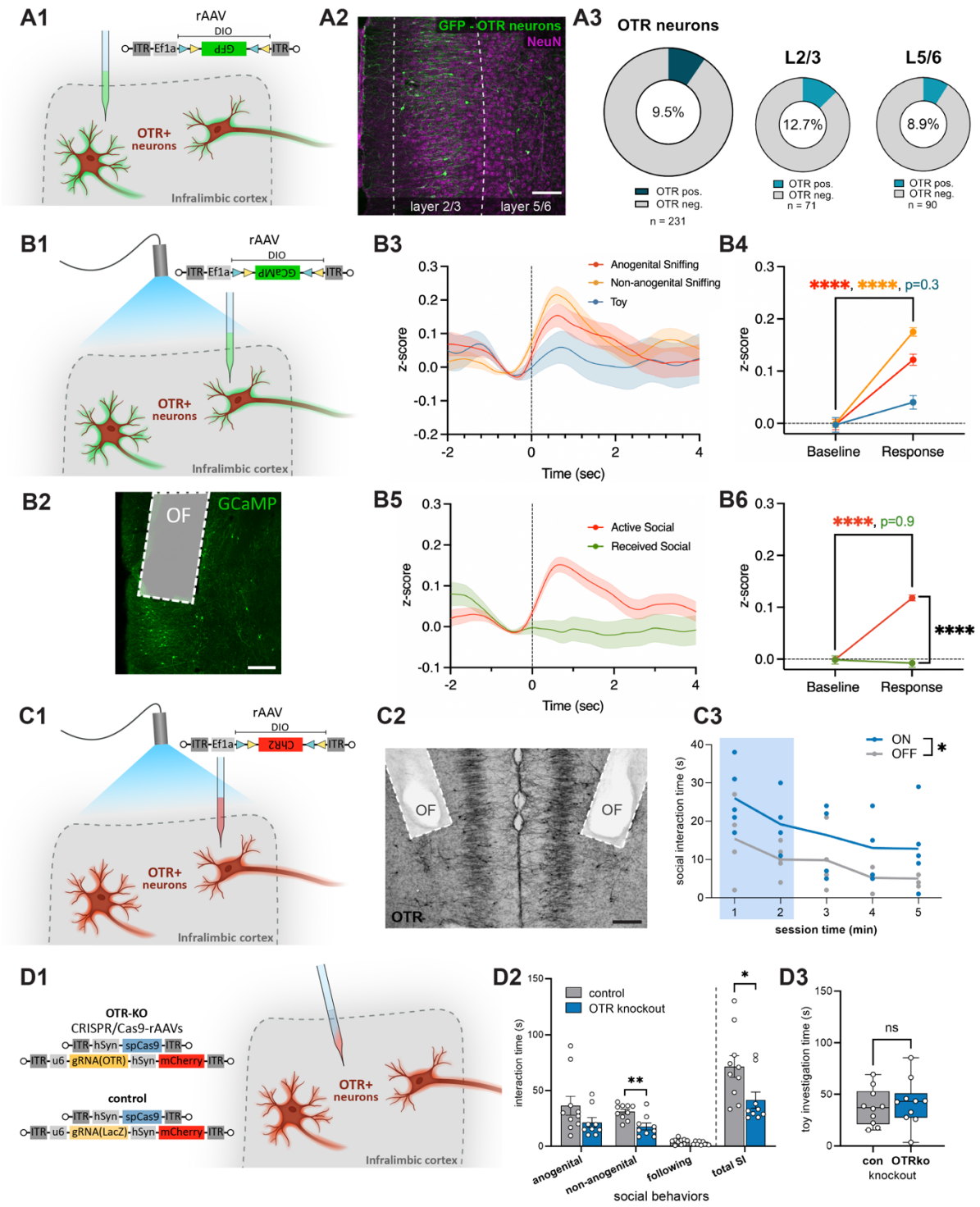

Figure 2 OTR neurons in the ILC are active during social behavior and modulate sociability

A OTR⁺ neurons in the ILC. **A1** Injection of an rAAV expressing GFP in a Cre-dependent manner and **A2** counterstaining for NeuN revealed that **A3** 9.5% of neurons in the ILC express OTRs, with very similar distributions in the superficial layers 2/3 and deeper layers 5/6. Scalebar 150µm.

B Recording of OTR⁺ neurons during social interaction. **B1** Injection of a rAAV expressing GCaMP6 in a Cre-dependent manner and implantation of an optic fiber into the ILC of OTR-Cre-rats to record Ca^{2+} activity from OTR⁺ neurons. **B2** Injection site showing OTR⁺ neurons infected with GCaMP (green) and the optic fiber (OF) tract. Scalebar 200µm. **B3** 1321 observations of neuronal activity during different social and non-social behaviors collected during several social interaction sessions in multiple animals (n=4) were aligned to the start of the behavior (t=0) and averaged per behavior (anogenital sniffing (n=391 events), non-anogenital

sniffing (n=706 events), toy investigation (n=224 events)). **B4** The strongest increase in intracellular calcium in OTR$^+$ neurons in the ILC was observed during anogenital and non-anogenital sniffing behavior, while the firing activity was not significantly increased during toy investigation compared to baseline activity. **B5** Neuronal activity during either active or received social interactions. **B6** Neuronal activity of OTR$^+$ neurons in the ILC was increased only during active social behaviors, but not during received social behaviors compared to baseline activity.
C Optogenetic activation of OTR$^+$ neurons in the ILC during social interaction. **C1** Injection of rAAV expressing the excitatory optogenetic channel Channelrhodopsin (ChR2) in a Cre-dependent manner into the ILC of female rats and implantation of an optic fiber above the ILC. **C2** Injection site showing OTR$^+$ neurons infected with ChR2 (black) and the optic fiber tract. Scalebar 200µm. **C3** Animals spend significantly more time socially interacting if the BL is ON in the first two minutes of the session, compared to when it is OFF (n=5 animals).
D Viral OTR knockout reduces social interaction. **D1** Injection of a virus system which utilizes CRISPR/Cas9 technology to specifically knockout OTRs locally in the ILC (n=9 animals knockout group, n=10 animals control group). **D2** OTR knockout significantly decreases social interaction (SI) time compared to control animals, especially for non-anogenital sniffing behavior. **D3** Investigation time of a toy rat in the open field remains unaltered by OTR knockout.

OTR$^+$ neurons in the ILC facilitate social behavior

To test whether activation of ILC OTR$^+$ neurons affects social behavior, we injected an rAAV expressing ChR2 in a Cre-dependent manner (rAAV-Ef1a-DIO-ChR2) into the ILC of OTR-Cre-rats and implanted optic fibers above the injection site **(Figure 2 C1-2)**. During the first 2 minutes of a 5-minute social interaction session, OTR$^+$ neurons were either activated by BL (30 Hz,10 ms pulses), or no light was applied for a baseline social behavior readout. Compared to the baseline, BL activation significantly increased social interaction times (average total interaction time per minute 17.5±8.6s vs 9.1±5.4s, p=0.013 two-way ANOVA) not only for the duration of the activation but throughout the whole session **(Figure 2 C3)**.

In order to verify that specifically OT signaling via OTRs contributes to this behavioral effect (as opposed to other potential receptors also expressed in OTR$^+$ neurons or pathways involving OTR$^+$ neurons), we introduced a discreet mutation in the OTR gene (Boender, Boon et al. 2023) **(Extended Data Figure S2D)** by injecting a mixture of two rAAVs expressing Cas9 (rAAV-hSyn-spCas9) and a guide RNA specific for the OTR-sequence (rAAV-u6-gRNA(OTR)-hSyn-mCherry), thus effectively depleting functional OTR expression. The control group received an rAAV for the expression of an unspecific guide RNA (rAAV-u6-gRNA(lacZ)-hSyn-mCherry) **(Figure 2 D1)**. Injection sites and viral expression were verified post-hoc **(Extended Data Figure S2C)**. We first confirmed the knockout of OTRs in the ILC functionally by bath application of the selective OTR agonist, TGOT, and *ex vivo* patch clamp electrophysiological recordings of OTR$^+$ neurons in both groups **(Extended Data Figure S2E)**. TGOT-induced membrane depolarization was significantly reduced by the viral OTR knockout compared to the control group **(Extended Data Figure S2F)**. During a free social interaction session with an unfamiliar conspecific, we observed that the OTR knockout significantly decreased interaction time (total social interaction time 71.5±31.1s vs 41.3±22.2s, p=0.028, two-way ANOVA). This effect was significantly driven by a decrease in non-anogenital sniffing (30.9±6.8 vs 17.6±9.4s p=0.0099, two-way ANOVA with Sidák's multiple comparison), while other behaviors, such as anogenital sniffing and following also showed a non-statistically significant decrease in time **(Figure 2 D2)**. Importantly, no difference was observed between the two groups when comparing their investigation time of a toy rat (37.7±18.0s vs 41.7±22.5s, p=0.67 unpaired t-test) **(Figure 2 D3)**. These experiments indicate that the increase of social interaction time depends specifically on OT/OTR signaling, rather than the release and activation of other neurotransmitters and receptors expressed in OTR$^+$ neurons.

OTRs are predominantly expressed in GABAergic neurons of the ILC

To further characterize the types of ILC OTR$^+$ neurons we employed a multiplex fluorescent in situ hybridization (RNAscope) approach **(Figure 3 A1-3)**, using probes for both OTR as well as Cre for verifying the specificity of our OTR-Cre rat line, as well as probes for vGlut1 (vesicular glutamate transporter), vGlut2 and vGAT1 (vesicular GABA transporter) to identify both glutamatergic and GABAergic neurons. Firstly, we showed that 94.8±2.7% of OTR-positive neurons were also Cre-positive, and vice versa 91.9±11.4% of Cre-positive neurons were also OTR-positive, confirming high specificity of the transgenic OTR-Cre line **(Figure 3 A4)**. Of all OTR-positive neurons, the vast majority co-expressed vGAT1 – a marker of GABAergic interneurons (93.32% vGAT1-positive), while only a small fraction co-expressed vGlut1 – a marker of glutamatergic neurons (3.34% vGlut1-positive), and none co-expressed vGlut2 **(Figure 3 A5)**. Interestingly, we observed distinct differences between the superficial and deeper layers of the ILC: OTR$^+$ neurons in layer 2/3 were exclusively GABAergic (100% vGAT1-positive) and showed higher OTR mRNA levels (as indicated by 9.1±1.7 puncta), while OTR$^+$ neurons in layer 5/6 were prevalently GABAergic (85.16% vGAT1-positive), but included a minority of glutamatergic neurons (7.42% vGlut1-positive) and exhibited lower OTR mRNA levels (3.8±1.3 and 4±0 average puncta, respectively) **(Figure 3 A6)**. To complementarily characterize the distinct glutamatergic and GABAergic OTR$^+$ populations in the ILC with a viral approach, we next injected both an rAAV labelling all OTR$^+$ neurons in red (rAAV-Ef1a-DIO-mCherry) as well as a second rAAV labelling all OTR$^+$ GABAergic interneurons (specificity achieved by DLX-enhancer (Dimidschstein, Chen et al. 2016)) in green (rAAV-DLX-DIO-GFP) into the ILC of female OTR-Cre rats **(Figure 3 B1)**. Similar to our findings with the RNAscope approach, we could identify an OTR$^+$ interneuron population in layer 2/3 (yellow) and an OTR$^+$ pyramidal population in layer 5/6 (red). Notably, we could also observe OT fibers throughout the ILC, with denser innervation in layer 2/3 **(Figure 3 B2)**. Together, these experiments demonstrate that the largest population of OTR$^+$ neurons in the ILC consists of GABAergic interneurons located in layer 2/3.

Histological quantification after viral labelling of OTR$^+$ cell types qualitatively confirmed that the majority of OTR$^+$ neurons were GAD-expressing interneurons immunopositive for parvalbumin and/or calbindin **(Extended Data Figure S3)**. Detailed anatomical imaging of cell bodies of OTR$^+$ neurons and OT fibers revealed the localization of OT-neuron axons in close proximity to OTR$^+$ neurons in different layers, further suggesting axonal release of OT activating OTR$^+$ neurons as indicated by our first experiments **(Figure 3 C1-3)**. In an *ex vivo* patch clamp experiment, where OTR$^+$ neurons were virally labelled by rAAV-Ef1a-DIO-GFP **(Figure 3 D1)**, both the large population of OTR$^+$ interneurons in layer 2/3 and the small population of OTR$^+$ pyramids in layer 5/6 **(Figure 3 D2)** fired extensively in response to 100nM TGOT bath application, confirming functional expression of OTR receptors in the virally labelled cell populations **(Figure 3 D3)**.

Figure 3

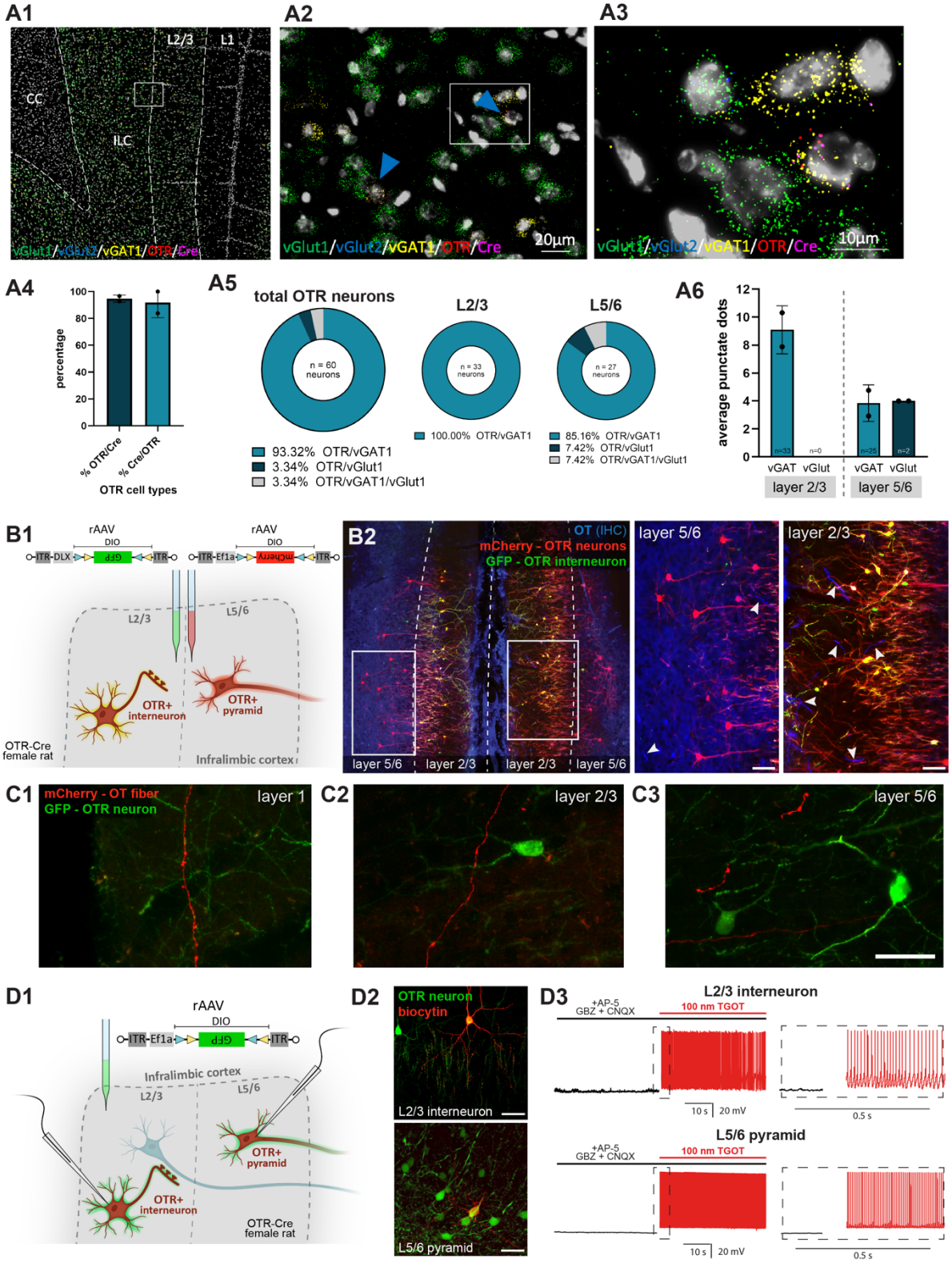

Figure 3 OTR⁺ cell types, their innervation by OT axons, and *ex vivo* responses to bath application of an OTR agonist
A RNAscope based characterization of OTR⁺ neurons in the ILC. **A1** Probes for vGlut1 (green), vGlut2 (blue), VGAT1 (yellow), OTR (red) and Cre (magenta) were applied to the ILC of female OTR-Cre rats. **A2-A3** Magnifications show representative vGAT1-positive neurons co-expressing Cre and OTR. **A4** Colocalization of OTR and Cre mRNA shows high specificity of the transgenic Cre rat line. **A5** The majority of OTR⁺ neurons in the ILC are GABAergic interneurons, with a small fraction of glutamatergic neurons, which are exclusively found in the layers 5/6. **A6** The GABAergic interneurons in layer 2/3 show a higher OTR mRNA density than those in the deeper layers 5/6.
B Morphologic characterization of OTR⁺ neurons in the ILC. **B1** Injection of a mixture of two rAAVs: one expressing mCherry in a Cre-dependent manner to label the entire population of OTR⁺ ILC neurons and a second rAAV expressing GFP in a Cre-dependent manner only in OTR⁺ interneurons (utilizing the DLX-enhancer for specific expression in interneurons) into the ILC of OTR-Cre female rats. **B2** OTR⁺ interneurons almost exclusively localized in layers 2/3 (yellow), OTR⁺ pyramidal neurons almost exclusively localized in layers 5/6 (red), with OT fibers (blue, white arrows) in both subdivisions of the ILC. Scalebar 50µm.

C OT fibers in close proximity to OTR$^+$ neurons. OT fibers stained immunohistochemically (red) are found **C1** close to the midline in layer 1, **C2** in close proximity to an OTR$^+$ interneuron in layer 2/3, and **C3** in close proximity to a pyramidal neuron in layer 5/6. Scalebar 40µm.
D *Ex vivo* electrophysiological characterization of OTR$^+$ neurons in the ILC. **D1** Injection of a rAAV expressing GFP in a Cre-dependent manner in OTR-Cre animals for the identification of OTR$^+$ neurons during *ex vivo* patch clamp recordings. **D2** Biocytin filled layer 2/3 interneuron and layer 5/6 pyramidal neuron. Scalebar 50µm. **D3** Representative traces of OTR$^+$ neurons firing upon bath application of an OTR agonist (TGOT) (n=4 rats for interneurons, n=2 rats for pyramidal neurons).

ILC OTR$^+$ interneurons promote both social interaction and social preference

Given the high numerical prevalence of OTR$^+$ interneurons, we aimed to investigate whether this specific OTR$^+$ cell population can induce similar behavioral effects as recruiting all ILC OTR$^+$ neurons **(Figure 2C)**. Therefore, we employed a rAAV equipped with the interneuron-specific enhancer DLX (Dimidschstein, Chen et al. 2016) to express Cre-dependent DREADDS (either hm3Dq(Gq) for activation or hM4Di(Gi) for inhibition) specifically in interneurons (rAAV-DLX-hm3Dq-GFP or rAAV-DLX-hm4Di-GFP) of the ILC of OTR-Cre female rats **(Figure 4 A1)**. Post-hoc IHC analysis verified the main population of OTR$^+$ interneurons being located in layer 2/3 **(Figure 4 A2)**. The two groups of rats (Gq: activation or Gi: inhibition) received CNO (3mg/kg) or saline i.p. injections 40 minutes before being introduced into a free social interaction session with an unknown conspecific, and the time of social interaction was scored. We found that chemogenetic activation of OTR$^+$ interneurons significantly increased social interaction time (61.5±17.7s saline vs 77.0±16.4s CNO, p=0.035 paired t-test), while chemogenetic inhibition significantly decreased social interaction time (61.0±16.6s saline vs 42.7±13.3s CNO, p=0.0197 paired t-test) **(Figure 4B)**. Notably, investigation of a toy rat was not altered by either activation or inhibition of OTR$^+$ interneurons (activation: 35.7±15.6s vs 40.8±19.7s, p=0.438 paired t-test; inhibition: 39.2±16.0s vs 49.0±28.5s, p=0.437 paired t-test). We also conducted a social novelty preference test with the animals to investigate whether OTR$^+$ interneuron action in the ILC has an effect on social memory. However, our findings showed no discernible difference in social novelty preference following chemogenetic activation of ILC OTR$^+$ interneurons **(Extended Data Figure S4A)**. These experiments confirmed that recruitment of ILC OTR$^+$ interneurons is sufficient to promote social behavior without alterations of social memory.

To further elucidate the social motivational aspect of the observed behavior, we analyzed whether manipulation of the OTR$^+$ interneuron population has an effect on social preference over other rewarding stimuli. Therefore, we subjected animals injected with the same chemogenetic excitatory rAAV system (rAAV-DLX-hm3Dq-GFP) to an adapted social vs food preference paradigm (Netser, Meyer et al. 2020) **(Figure 4 C1)**, where in a satiated state animals are expected to highly prefer social interaction, while food restriction for 24 hours leads to a shift of preference towards food **(Extended Data Figure S4 B1-2)**. In baseline conditions (saline i.p. 40 minutes before session) we observed the expected social preference at satiety (0.37±0.21) with a significant shift towards food preference after 24h of food deprivation (-0.40±0.19) (p<0.0001, repeated measures one-way ANOVA with Sidák's multiple comparison) **(Figure 4 C2)**. At satiety, chemogenetic activation (CNO i.p. 40 minutes before session) had no significant effect on the social preference (0.48±0.13, p=0.8114), indicating a ceiling effect with cornered social interaction. After 24h of food deprivation however, chemogenetic activation of OTR$^+$ interneurons in the ILC significantly increased the social preference, even shifting from a clear preference for food to a slight preference for social interaction (0.02±0.24, p=0.0059). Notably, this effect was driven by an increased number of bouts (number of visits to the social corner) at 24h of food deprivation after CNO injection **(Figure 4 C3)**, while the length of bouts (average length per visit of the

social corner) (Figure 4 C4) and the number of transitions between the two corners (Extended Data Figure S4 B3) remained unaltered. Altogether these findings suggest that OTR$^+$ interneurons selectively promote social preference even under conditions of mild starvation.

Figure 4

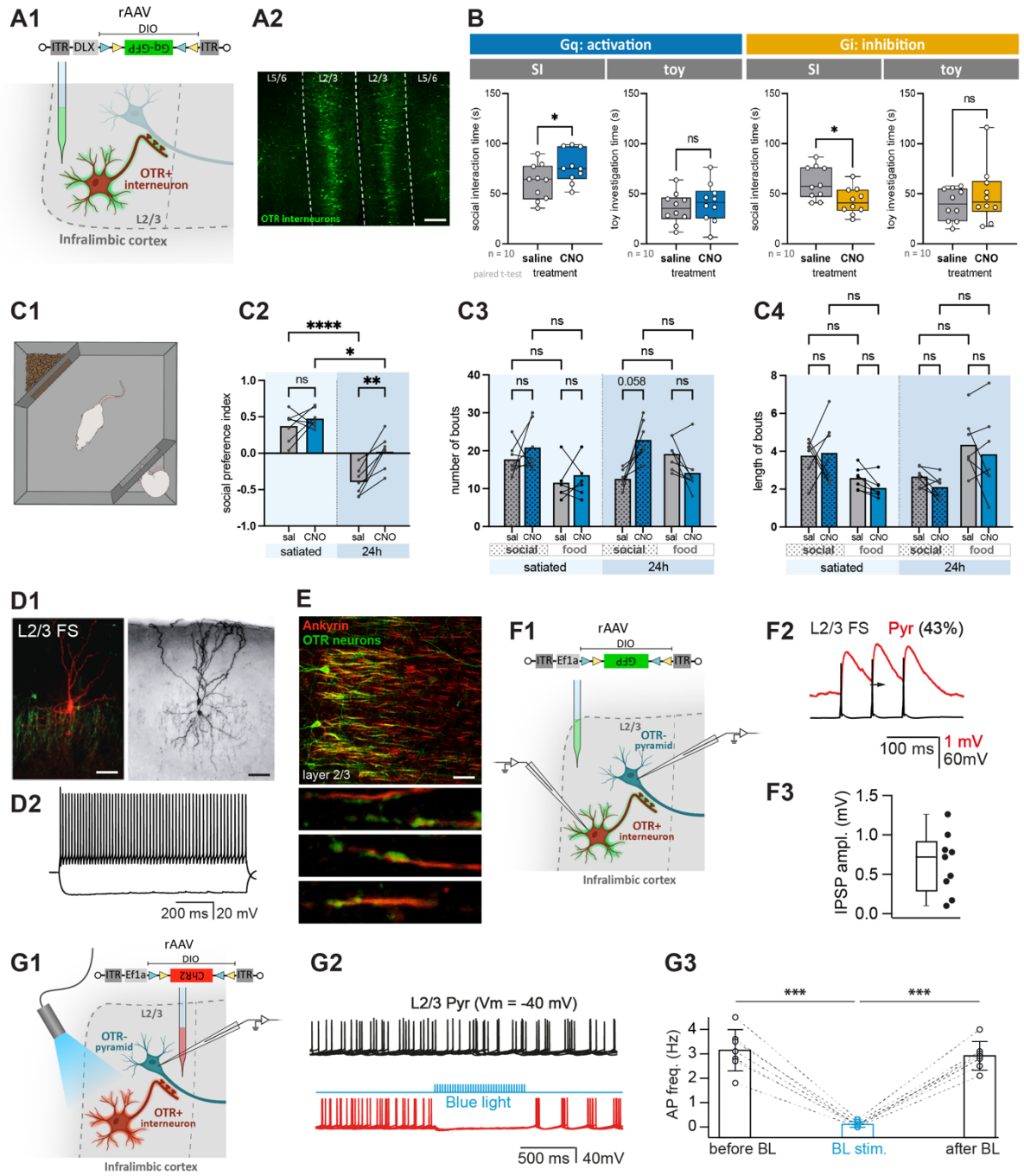

Figure 4 OTR$^+$ interneurons modulate social behavior and social preference

A Chemogenetic manipulation of OTR$^+$ interneurons in the ILC. **A1** Injection of a rAAV expressing the excitatory (Gq) or inhibitory (Gi) DREADD (designer receptor exclusively activated by designer drugs) in a Cre-dependent manner in all OTR$^+$ interneurons (via DLX enhancer) in the ILC of transgenic OTR-Cre female rats. **A2** Injection site showing localization of OTR$^+$ interneurons (green) in layer 2/3.

B Chemogenetic manipulation of OTR$^+$ interneurons via CNO injection before a 5 min social interaction (SI) session with an unknown conspecific in the open field. Activation (n=10 animals) or inhibition (n=10 animals) of OTR interneurons significantly increases or decreases social interaction time, respectively. Investigation time of a toy rat in the open field remains unaltered by chemogenetic manipulation.

C1 The social vs food preference paradigm is performed in an open field arena with the addition of two triangular dividers in opposite corners with a front mesh. The mesh allowed for indirect interaction with an unknown social partner (only sniffing or hearing) but no direct social touch, or investigation of food pellets (only sniffing) without eating them. **C2** Chemogenetic activation of OTR$^+$ interneurons increases social preference (measured via the social preference index) after 24h of food deprivation (n=7 animals). **C3** This effect is driven by an increase in the number of bouts rather than **C4** the length of bouts.

D Morphological and functional characterization of OTR$^+$ chandelier neurons. **D1** Fluorescent (left) and DAB (right) staining of a biocytin-filled OTR$^+$ ILC neuron reveal the morphological features of chandelier neurons bearing vertically aligned axonal cartridges. **D2** Representative *ex-vivo* recording of OTR$^+$ chandelier interneuron showing its fast-spiking (FS) activity.
E Ankyrin staining (red, marker for axon-initial segments) reveals the close proximity of OTR$^+$ boutons (green, viral labelling) to the initial segment of the axon of the local OTR-negative (OTR$^-$) pyramidal neurons.
F Paired patch-clamp recordings of OTR$^+$ fast-spiking (FS) interneurons. **F1** A Cre-dependent GFP-expressing rAAV was injected into the ILC of OTR-Cre rats to characterize OTR$^+$ neurons; an ex vivo paired patch clamp experiment was performed, where OTR$^+$ interneurons (green) were stimulated while the activity of OTR$^-$ pyramidal neurons (no fluorescent marker) was recorded. **F2** A representative paired recording shows stimulation of the layer 2/3 FS OTR$^+$ interneuron (black) and the evoked postsynaptic potential of an OTR$^-$ pyramidal neuron (red). **F3** Inhibitory post-synaptic potential (IPSP) amplitude of OTR$^-$ pyramids after stimulation of OTR$^+$ interneurons (number of tested pairs: 21, number of connected pairs: n = 9, brain slices obtained from 3 rats).
G *Ex vivo* optogenetic stimulation of OTR$^+$ interneurons and patch clamp recording of OTR$^-$ pyramidal neurons. **G1** A Cre-dependent ChR2-expressing rAAV was injected into the ILC of OTR-Cre rats, in order to activate OTR$^+$ neurons upon BL stimulation; an *ex vivo* patch clamp experiment was performed, where OTR$^+$ neurons (red) were stimulated with BL while the activity of OTR$^-$ pyramidal neurons (no fluorescent marker) was recorded. **G2** Representative traces of a layer 2/3 OTR$^-$ pyramidal neuron at baseline (black) and during BL stimulation of OTR$^+$ neurons (red). **G3** Action potential frequency (AP freq.) of inhibited OTR$^-$ pyramids before, during, and after optogenetic stimulation of OTR$^+$ neurons (n = 7 cells, brain sections were obtained from 2 rats).

OTR$^+$ fast-spiking interneurons inhibit pyramidal neurons in the ILC

To further characterize the most abundant type of ILC OTR$^+$ interneurons we performed an *ex vivo* filling with biocytin, which allowed us to conclude that the vast majority of the recorded OTR$^+$ cells exhibited axonal arborization with characteristic features of axo-axonic interneurons (chandelier neurons) (Somogyi 1977) **(Figure 4 D1)**. In addition, the majority (83%, n=24 patched cells, slices obtained from 5 rats) of OTR$^+$ interneurons in layer 2/3 showed fast-spiking firing patterns in response to prolonged depolarizing current injection typical for this type of GABAergic interneurons. **(Figure 4 D2)** (Freund and Gulyás 1996). Bath application of TGOT at both low and high concentrations (20nM and 100nM, respectively) during *ex vivo* patch clamp recordings reliably and significantly increased their firing activity. Note that although the percentage of responding cells did not depend on the TGOT concentration, the average firing rate was twice as high at higher agonist concentrations **(Extended Data Figure S4C)**. Furthermore, IHC staining for ankyrin (a marker for the axon initial segment) revealed that the terminals of axon arbors of the OTR$^+$ neurons form distinct arrays (so-called "cartridges") along the axon initial segments of OTR-negative (OTR$^-$) pyramids **(Figure 4E)**. These morphological and functional features of chandelier neurons were observed in the majority of OTR interneurons in layer 2/3 of the ILC.

To functionally test whether OTR$^+$ interneurons in layer 2/3 inhibit OTR$^-$ pyramidal neurons, we first performed single-cell based *ex vivo* paired patch-clamp recordings. Three weeks following an injection of a rAAV expressing GFP in a Cre-dependent manner into the ILC (rAAV-Ef1a-DIO-GFP), fluorescently labelled OTR$^+$ neurons were stimulated *ex vivo* while non-fluorescent OTR$^-$ pyramidal neurons were recorded **(Figure 4 F1-2)**. The results demonstrated that stimulation of the presynaptic OTR$^+$ interneurons led to the induction of an inhibitory post-synaptic potential in 43% of tested pairs **(Figure 4 F3)**, further corroborating the inhibitory nature of the synaptic connection of OTR$^+$ neurons in layer 2/3 targeting OTR-negative pyramidal neurons. In a follow-up *ex vivo* patch clamp experiment we recorded spontaneous excitatory (EPSC) and inhibitory (IPSC) post-synaptic currents in layer 2/3 OTR$^-$ pyramidal neurons. The bath application of TGOT significantly increased the IPSC amplitude, with no effect on EPSC amplitude or EPSC and IPSC frequency **(Extended Data Figure S4D)**. Additionally, we also applied a population-based *ex vivo* approach, utilizing optogenetic stimulation of ChR2-expressing OTR$^+$ neurons (in rAAV-Ef1a-DIO-ChR2-mCherry ILC injected OTR-Cre rats) while simultaneously recording local OTR$^-$ pyramidal neurons **(Figure 4 G1)**. Consistent with the results of

the paired recordings and the effect of TGOT application on IPSC amplitude observed in the OTR$^-$ pyramids, BL stimulation resulted in a significant decrease of action potential frequency of the local output pyramidal neurons **(Figure 4 G2-3)**. Thus, together these experiments suggest that endogenous OT release in the ILC first activates layer 2/3 OTR$^+$ interneurons, which in turn inhibits OTR$^-$ down-streaming principal cells located in the same layer of the ILC.

OTR$^+$ interneurons inhibit the ILC–basolateral amygdala pathway

Having established the targeted inhibitory input from OTR$^+$ interneurons to layer 2/3 OTR$^-$ pyramidal neurons, our next objective was to investigate the potential downstream projection sites of those principal cells. Therefore, we analyzed the neuronal activity marker cFos expression in seven pre-selected brain regions downstream to the ILC (Gabbott, Warner et al. 2005), which were also reported to be functionally involved in modulation of social behaviors (Ko 2017), upon the experimental CNO-triggered activation of rAAV-DLX-DIO-Gq-GFP infected OTR$^+$ interneurons in the ILC. While control animals receiving saline injections showed no specific cFos expression in OTR$^+$ interneurons (0.69±0.37 % cFos/GFP double-positive cells, n=375 GFP$^+$ neurons from 3 animals), animals receiving CNO showed cFos signal in these GFP+ cells (99.91±0.15 % cFos/GFP double-positive cells, n=424 GFP$^+$ neurons from 3 animals) **(Figure 5 A1)**. To allow for unbiased quantification of neuronal cFos expression, we employed a fully automated pipeline based on the Imaris software which analyzed cFos signals in more than 500,000 neurons across the seven different brain regions. Activating OTR$^+$ inhibitory interneurons in the ILC resulted in an overall decrease of cFos expression in the ILC **(Figure 5 A2)**, indicating extensive inhibition of OTR(GFP)-negative principal cells **(Figure 4G)**. As for the analyzed downstream regions, cFos expression was not significantly changed in the periaqueductal grey (PAG), lateral septum, supramammillary nuclei (Summ), or ventral tegmental area (VTA), however, it was significantly reduced in the basolateral amygdala (BLA) **(Figure 5 A2)**. This suggests that experimental OT release in the ILC ultimately reduces the activity of BLA neurons. Notably, in the same paradigm, we observed a significant increase in cFos expression in the nucleus accumbens (NAc), hinting at differences between the possible functional dichotomy of BLA and NAc projections from the ILC. This suggests that ILC output neurons projecting to the NAc are not directly (monosynaptically) inhibited by layer 2/3 OTR$^+$ interneurons.

To test this hypothesis, we performed viral retrograde tracing of neurons projecting to the BLA or to the NAc by injection of a retrograde GFP-expressing rAAV (retro-rAAV-hSyn-GFP) into either BLA or NAc. The same animals were injected into the ILC with a Cre-dependent rAAV expressing mCherry in interneurons (rAAV-DLX-DIO-mCherry) to visualize the overall topography of back-labeled projecting cells in the ILC in relation to the OTR$^+$ cell population **(Figure 5 B1, C1)**. Injection sites in the BLA or NAc were marked by co-injection of a small amount of soluble fluorescent beads in the tip of the injection pipette **(Extended Data Figure S5 A)**. A substantial number of BLA-projecting neurons was found within the “inhibitory sleeve” in layer 2/3 **(Figure 5 B2)** as well as in the deeper layers of the ILC. In contrast, retrogradely labeled NAc-projecting neurons were found exclusively in the deeper layers of the ILC, but not within the “inhibitory sleeve” of layer 2/3 **(Figure 5 C2)**. Furthermore, detailed morphological analysis of BLA-projecting neurons revealed that OTR$^+$ interneurons form direct axo-axonic contacts with BLA-projecting pyramidal neurons in layer 2/3 (**Figure 5D**), but not with NAc-projecting pyramidal neurons in layer 5/6.

Figure 5

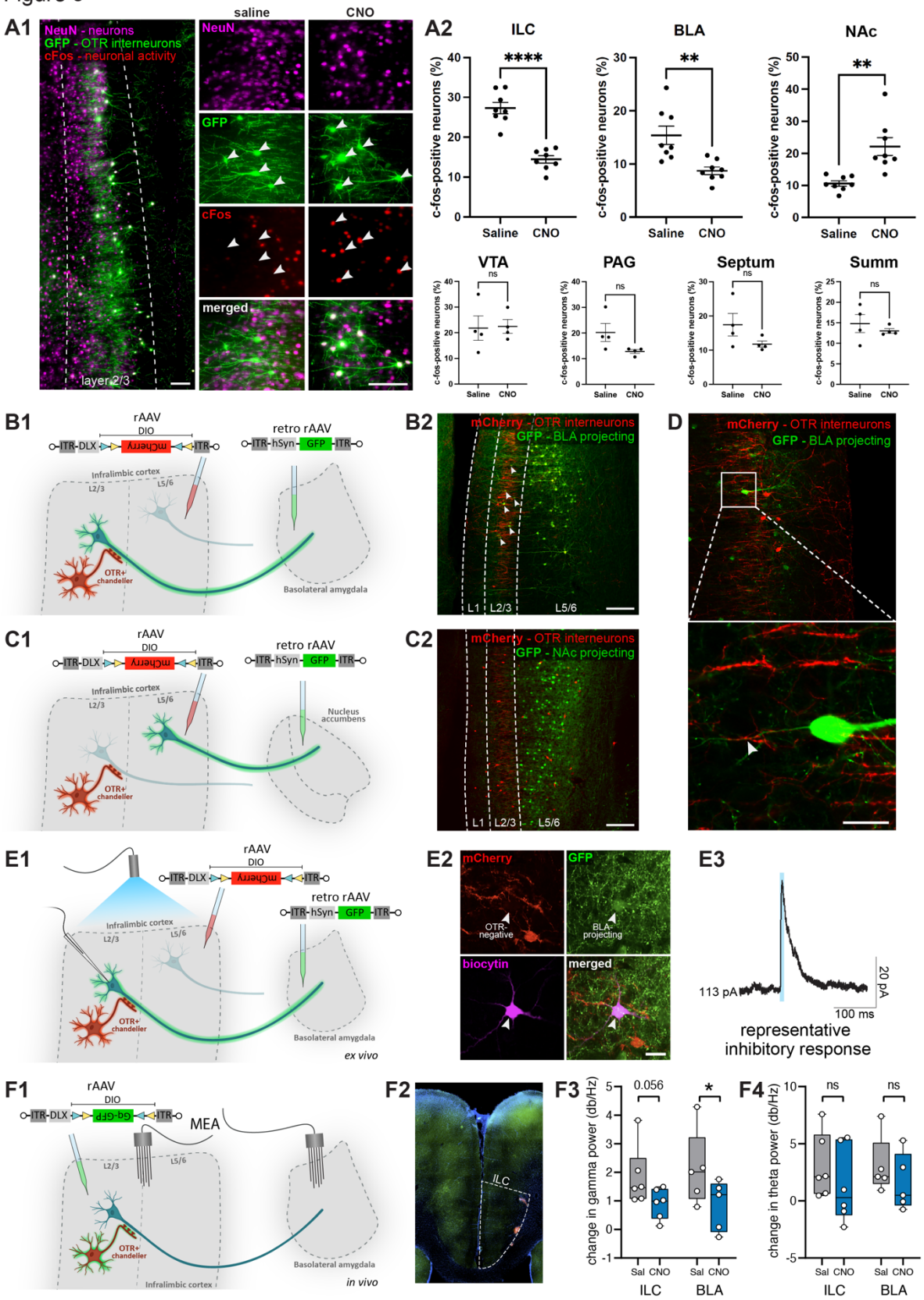

Figure 5 OTR⁺ interneurons modulate neuronal activity in the BLA

A Expression of cFos after chemogenetic activation of OTR⁺ interneurons in the ILC. **A1** A rAAV expressing GFP-Gq (excitatory DREADD) in all OTR⁺ interneurons (green) was injected into the ILC of female rats; after either CNO or saline administration followed by perfusion (100 minutes post injection) brain sections were immunohistochemically stained for NeuN (magenta) and cFos (as a marker for neuronal activity, red). After CNO injection, OTR⁺ interneurons were activated chemogenetically as verified by cFos expression (white arrows), whereas after saline injection only baseline cFos expression occurred with no cFos expression in OTR⁺ interneurons (white arrows). Scalebar 100µm **A2** Local reduction of cFos expression in the ILC after chemogenetic activation of OTR⁺ interneurons in the ILC. Local reduction or increase of cFos expression in the BLA or NAc, respectively, after chemogenetic activation of OTR⁺ interneurons in the ILC. No significant change of cFos expression was observed in the VTA, PAG, septum, or Summ (brain sections were obtained from n=8 animals per group).

B Retrograde tracing of BLA-projecting neurons in the ILC. **B1** Injection of a retrogradely GFP-expressing rAAV into the BLA with simultaneous injection of a Cre-dependent mCherry-expressing interneuron-specific rAAV into the ILC. **B2** BLA-projecting neurons are found both within layer 5/6, as well as within in the inhibitory sleeve of OTR$^+$ interneurons in layer 2/3 (white arrows). Scalebar 200µm.
C Retrograde tracing of NAc-projecting neurons in the ILC. **C1** Injection of a retrogradely GFP-expressing rAAV into the NAc with simultaneous injection of a Cre-dependent mCherry-expressing interneuron-specific rAAV into the ILC. **C2** NAc-projecting neurons are found only within layer 5/6, but not within the inhibitory sleeve of layer 2/3. Scalebar 200µm.
D Representative axo-axonic contact (white arrow) of OTR$^+$ interneuron (red) on BLA-projecting pyramidal neuron (green). Scalebar 20µm.
E Electrophysiological patch-clamp recording of OTR$^-$ neurons projecting to the BLA. **E1** Injection of an rAAV expressing ChR2 in a Cre-dependent manner in OTR$^+$ interneurons of OTR-Cre animals, with additional injection of an rAAV into the BLA for retrogradely identifying projecting neurons. During an *ex vivo* patch clamp recording of BLA-projecting neurons, BL is used to activate OTR$^+$ interneurons. **E2** Representative image of a biocytin-filled OTR$^-$ BLA-projecting pyramidal neuron. Scalebar 20µm. **E3** Representative averaged trace of a whole-cell patch clamp recording (voltage clamp, holding voltage -60mV) depicting an inhibitory response of a BLA-projecting neuron within the inhibitory sleeve (layer 2/3) after optogenetic activation of OTR$^+$ interneurons in the ILC (n=11 recorded neurons).
F In vivo electrophysiological LFP recordings of ILC and BLA. **F1** An rAAV expressing GFP-Gq (excitatory DREADD) in all OTR$^+$ interneurons (green) was injected into the ILC of female rats; MEA were implanted into the ILC and BLA. Prior to the food vs. social task, animals were either injected with CNO or saline. **F2** Horizontal brain section showing OTR$^+$ interneurons (green) in the ILC and electrode tracts (red). **F3** Change in gamma power but no **F4** change in theta power in the ILC and BLA compared to baseline (no social or food stimuli present) is reduced after CNO administration (n=6 animals).

Following this clear anatomical distinction, we next verified inhibitory action of ILC OTR$^+$ interneurons on OTR$^-$ pyramidal neurons projecting to the BLA. In the first set of experiments, both a retrograde rAAV expressing GFP was injected into the BLA (retro-rAAV-hSyn-GFP) and a Cre-dependent rAAV expressing ChR2 in interneurons (rAAV-DLX-DIO-ChR2-mCherry) into the ILC of OTR-Cre-rats. After a 3-week expression period, OTR$^+$ interneurons were optogenetically activated by BL stimulation in an *ex vivo* experimental setup, while BLA-projecting OTR$^-$ pyramids were recorded in whole cell mode **(Figure 5 E1)**. Neurons were patched only if they were both GFP-positive (BLA-projecting) and mCherry-negative (OTR$^-$ neurons) **(Figure 5 E2)**. Recorded neurons were identified as principal cells based on their typical discharge pattern and morphology after filling with biocytin and post-recording staining procedure **(Extended Data Figure S5 B** and **Figure 5 E2)**. Notably, all recorded neurons (n=11) responded with inhibition to BL induced OTR$^+$ interneuron activation (**Extended Data Figure S5 C** for responses of BLA-projecting OTR$^-$ pyramids, **Extended Data Figure S5 D** for representative trace verifying activation of OTR+ interneuron by BL). A representative response of a BLA-projecting OTR$^-$ pyramid is depicted in **Figure 5 E3**.

In the next set of experiments, we performed simultaneous recordings of local field potentials (LFPs) using custom-made microelectrode arrays (MEAs; **Extended Data Figure S5 E1**) (Mohapatra, Netser and Wagner 2022) from the ILC and BLA **(Extended Data Figure S5 E2-3)** of freely moving rats after selective activation of OTR$^+$ interneurons in the ILC **(Figure 5 F1-2)**. Three weeks after injection of an rAAV expressing hM3Dq-GFP in a Cre-dependent manner in interneurons (rAAV-DLX-DIO-Gq-GFP) and seven days after MEA implantation, adult female OTR-Cre rats were recorded while conducting the social vs. food task at satiety. LFP signals were analyzed across the 5-min baseline period before stimuli introduction and the 5-min encounter period after stimuli introduction. We found no difference between CNO and saline injection in theta or gamma power of the LFP signals recorded during the baseline period **(Extended Data Figure S5 F1-2)**. Introduction of a social stimulus following the baseline period increased gamma and theta power (as can be observed by a positive change in power in **Figure 5 F3-4**). However, we observed a significant reduction in the change in power of gamma, but not theta LFP oscillations recorded during the encounter after CNO injection, as compared to saline injection **(Figure 5 F3-4)**. This reduction was observed in both the ILC and BLA (p = 0.017 for treatment in two-way ANOVA; p = 0.056 for ILC, p = 0.045 for BLA in paired t-test). In conclusion, both *ex vivo* and *in vivo*

results provide evidence that the activation of ILC OTR axo-axonic interneurons primarily inhibits the ILC-BLA pathway.

DISCUSSION

Our study demonstrates that OT release within the mPFC directly facilitates social behaviors in female rats. We found that the ventral part of the mPFC, especially its ILC subdivision, is preferentially innervated by OT neurons. Therefore, we propose that OT action within the rat mPFC is particularly strong in the ILC. Indeed, targeted experimental release of OT in the ILC by optogenetic stimulation increased social interactions between female rats. These findings are consistent with previous studies indicating the involvement of OT in the modulation of social behavior through its actions in various brain regions (Marlin and Froemke 2016, Grinevich and Stoop 2018). Our results extend these observations by specifically implicating the ILC in the PVN-to-PFC OT signaling pathway (Liu, Li et al. 2023), revealing its role in facilitating social interactions. The observed increase in social behaviors upon optogenetic stimulation of hypothalamic OT neurons (Lee, Rhim et al. 2016, Tang, Benusiglio et al. 2020) supports the role of OT in promoting social motivation and interaction.

We further established that OTR^+ neurons in the ILC are intrinsically active during social behavior, with activity specific to interaction events initiated by the test rat compared to ones initiated by the social partner (e.g., sniffing vs being sniffed). The differential activation of OTR^+ ILC neurons during active versus received social behaviors suggests a role for these neurons as initiators of social interaction. This may further indicate that OTR^+ neurons in the ILC play a pivotal role in the decision making processes underlying social executive functions of the mPFC (Kingsbury, Huang et al. 2019). Our results convincingly demonstrate that OT action in the ILC facilitates sociability via axonal OT release (Knobloch, Charlet et al. 2012).

We further explored the local ILC neuron circuit receptive to OT using our multiplex fluorescent in situ hybridization data and neuroanatomical analyses. Our findings revealed that the vast majority of OTR^+ neurons in the ILC are GABAergic interneurons, located predominantly in layers 2/3. Further investigation based on characteristic morphological and electrophysiological features showed that a large proportion of OTR^+ neurons belong to the class of inhibitory interneurons called axo-axonic cells (also known as chandelier cells), which are known to be powerful inhibitors of output principal cells in cortical circuits (Jung, Choi and Kwon 2022). Among GABAergic interneurons, axo-axonic cells are unique in that they form synapses with the axon initial segment of pyramidal neurons, where action potentials are generated. This unique inhibitory efficacy of chandelier cells enables their precise control over the activity of output pyramidal neurons and overall network excitability. The functional activation of these interneurons led to significant behavioral changes, suggesting that GABAergic modulation within the ILC is crucial for social behavior regulation. This finding is consistent with the known role of GABAergic interneurons in shaping cortical output and influencing behavior (Yang, Mack et al. 2021).

In particular, the observed shift from food preference (an appetitive non-social stimulus) to social stimuli following an artificial increase in the value of food through a 24h food restriction is consistent with the hypothesis of mutually inhibitory ensembles in the mPFC (Gangopadhyay, Chawla et al. 2021). In line with their hypothesis and based on our results, we speculate that social decision making is facilitated by specific neuronal ensembles within the ILC that are selectively activated by social stimuli and modulated by OT action. Thus, specific OTR^+ interneurons within the ILC promote social behavior and contribute to the encoding of socially relevant information and biasing decisions toward prosocial behaviors. In contrast, certain non-social ILC ensembles are activated by non-social stimuli and are

involved in processing individual-centric information. In our study, food deprivation might increase the strength of inhibition of the non-social ensemble, leading to a preference of food in the food restricted baseline condition. An increase in OTR$^+$ interneuron signaling in the ILC might however strongly inhibit the non-social ensembles, thus lifting the inhibition of the social ensemble and shifting the balance away from food preference (Gangopadhyay, Chawla et al. 2021).

We further sought to investigate downstream regions being targeted by the ILC layer 2/3 principal cells that are subject to inhibition by OTR$^+$ interneurons. We chose to analyze the BLA and the NAc, two areas that are well-known to be involved in socially relevant functions including fear, reward, and social interaction(Gabbott, Dickie et al. 1997, Gabbott, Warner et al. 2005, Bloodgood, Sugam et al. 2018). Chemogenetic activation of OTR$^+$ ILC neurons in our experiment led to downregulation of cFos expression in the BLA and increased cFos expression in the NAc. We propose that the substantial reduction in the number of cFos-positive cells in the BLA observed in our paradigm is caused by the reduction of excitatory input to the BLA from ILC principal cell projections that are being inhibited by local ILC OTR$^+$ interneurons. Among the mPFC subdivisions, the ILC in particular is known to target a dense population of GABAergic interneurons in the BLA (Davis, Zaki et al. 2017) and the BLA in turn densely innervates the NAc (Correia, McGrath et al. 2016). We hypothesize that the observed cFos upregulation in the NAc might be caused by the suppression of BLA interneuron activity, thereby increasing the excitatory signaling from the BLA to the NAc. Although, the approach of investigating circuits via cFos activity patterns comes with the caveat of spatial and temporal ambiguity. Therefore, we further investigated the OTR-ILC-BLA/NAc circuit both anatomically and electrophysiologically. Retrograde tracing following injections in the BLA and NAc revealed BLA-projecting principal cells in the ILC that were embedded within a dense “inhibitory sleeve” formed by the vertical axonal cartridges of OTR$^+$ chandelier cells. Additionally, we showed OTR$^+$ interneurons forming axonal cartridges at the initial axonal segment of neurons projecting to the BLA, which was not observed in the case of NAc-projecting pyramids. This observation was further confirmed by *ex vivo* studies which showed direct monosynaptic coupling between OTR$^+$ interneurons and BLA-projecting principal cells. Furthermore, our *in vivo* LFP recordings showed a decrease in social-behavior-associated gamma power change in the BLA after OTR$^+$ interneuron stimulation in the ILC. Since activation of the ILC-BLA circuit during fear memory recall is associated with increased gamma oscillations (Courtin, Karalis et al. 2014), the reduction in gamma power observed by us following ILC OTR$^+$ interneuron activation suggests a reduced activity in this circuit, which is in accordance with our cFos results **(Figure 5A)**. These observations support the conclusion that specifically targeted inhibition of BLA-projecting pyramidal neurons appears to be driven by OTR$^+$ interneurons, thus further solidifying this downstream-projecting neuronal population as the main ensemble facilitating the observed behavioral effects.

We acknowledge the possibility that other OT-dependent pathways involved in various behaviors originate from the PFC. There are reports that principal neurons in the PFC are sensitive to bath application of OT (Ninan 2011) or express OTRs (Tan, Singhal et al. 2019), the latter also being shown in a small fraction of OTR$^+$ neurons by our in situ hybridization data and viral labelling. In mice, numerous OT-sensitive principal cells can be found throughout the entire mPFC, including the infralimbic area (Newmaster, Nolan et al. 2020), and they are located in both superficial and deeper layers. On the contrary, our results in rats report considerably fewer (7% in situ hybridization data, **Figure 3A**) principal cells that express OTRs and these cells are located exclusively in the deeper

layers, particularly outside of the layer 2/3 “inhibitory sleeve” **(Figure 3B)**. This may explain why we did not observe social memory alterations following the activation of OTR^+ interneurons **(Extended Data Figure S4A)** as previously found in male mice after manipulation of the direct PFC-BLA pathway (Tan, Singhal et al. 2019). In addition to the differences in species and sex, Tan and colleagues showed that these principal OTR^+ neurons specifically alter social memory, while having no particular effect on general sociability. This could indicate the existence of two independent, distinct, and potentially species- and sex-dependent OT-modulated pathways for sociability (interneurons) and social memory (pyramidal neurons). A distinctive organization of the OT systems in different mammals, including mice and rats, has been identified at the anatomical and behavioral level (Insel, Gingrich and Young 2001, Freeman and Young 2016, Althammer, Jirikowski and Grinevich 2018), reflecting species-dependent processing of social information and subsequent selection of optimal social strategy (Young 1999, Bielsky and Young 2004, Anacker and Beery 2013, Burkett, Andari et al. 2016).

In conclusion, our study identifies a critical role for OT signaling within the ILC in facilitating social behaviors in female rats **(Extended Data Figure S5 G)**. Activation of GABAergic OTR^+ interneurons in particular appears to play a significant role in modulating social interaction. These findings contribute to our understanding of the neural mechanisms underlying social behavior and highlight the potential of targeting OT pathways for therapeutic interventions in social deficits (Meyer-Lindenberg, Domes et al. 2011), as the PVN-to-PFC OT signaling pathway is conserved throughout evolution and exists in several primate species including humans (Rogers, Ross et al. 2018, Lefevre, Meza and Miller 2024).

Acknowledgments

We thank Andreas Draguhn for his input on electrophysiological experiments, Laura Dötsch for performing the Western blot experiment, Selina Wunsch for assisting in the cFos quantification, and Quirin Krabichler and Jonas Schimmer for technical assistance with virus injections. This work was supported by a PhD scholarship of the Studienstiftung des Deutschen Volkes to SS, Marie Sklodowska-Curie fellowship (101018877) to AL, DFG Emmy Noether starting grant AL 2466/2-1 to FA, the Synergy European Research Council (ERC) grant “OxytocINspace” 101071777 to VG, SFB Consortium 1158-3 to VG, and German-Israeli Project cooperation (DIP) GR3619-1 to RH, VG and SW.

Authors contribution

Project conception: ME, VG. Anatomical experiments: ME, SS, FA, TS, YP. Behavioral experiments (optogenetic/chemogenetic): SS, AL, ARa. Ex vivo patch-clamp electrophysiology: AK, JL, ARo, KA, DH, SM, HM. In vivo fiber photometry: AL, RP, AS. In vivo electrophysiology (MEA): RT, SN. RNAscope: AK, AG, AT, AB. Methodology: SS, AB, AL, RH. Project administration and supervision: SW, ME and VG. Funding acquisition: VG.

REFERENCES

Althammer, F., G. Jirikowski and V. Grinevich (2018). "The oxytocin system of mice and men—similarities and discrepancies of oxytocinergic modulation in rodents and primates." Peptides **109**: 1-8.

Anacker, A. M. and A. K. Beery (2013). "Life in groups: the roles of oxytocin in mammalian sociality." Frontiers in behavioral neuroscience **7**: 185.

Bielsky, I. F. and L. J. Young (2004). "Oxytocin, vasopressin, and social recognition in mammals." Peptides **25**(9): 1565-1574.

Bloodgood, D. W., J. A. Sugam, A. Holmes and T. L. Kash (2018). "Fear extinction requires infralimbic cortex projections to the basolateral amygdala." Translational psychiatry **8**(1): 60.

Boender, A. J., M. Boon, H. E. Albers, S. R. Eck, B. A. Fricker, A. M. Kelly, J. E. LeDoux, S. C. Motta, P. Shrestha and J. H. Taylor (2023). "An AAV-CRISPR/Cas9 strategy for gene editing across divergent rodent species: Targeting neural oxytocin receptors as a proof of concept." Science Advances **9**(22): eadf4950.

Bruno, C. A., C. O'Brien, S. Bryant, J. I. Mejaes, D. J. Estrin, C. Pizzano and D. J. Barker (2021). "pMAT: An open-source software suite for the analysis of fiber photometry data." Pharmacology Biochemistry and Behavior **201**: 173093.

Burkett, J. P., E. Andari, Z. V. Johnson, D. C. Curry, F. B. M. de Waal and L. J. Young (2016). "Oxytocin-dependent consolation behavior in rodents." Science (New York, N.Y.) **351**(6271): 375-378.

Calcagnoli, F., C. Stubbendorff, N. Meyer, S. F. de Boer, M. Althaus and J. M. Koolhaas (2014). "Oxytocin microinjected into the central amygdaloid nuclei exerts anti-aggressive effects in male rats." Neuropharmacology.

Chini, B., M. Verhage and V. Grinevich (2017). "The Action Radius of Oxytocin Release in the Mammalian CNS: From Single Vesicles to Behavior." Trends in Pharmacological Sciences.

Correia, S. S., A. G. McGrath, A. Lee, A. M. Graybiel and K. A. Goosens (2016). "Amygdala-ventral striatum circuit activation decreases long-term fear." Elife **5**: e12669.

Courtin, J., N. Karalis, C. Gonzalez-Campo, H. Wurtz and C. Herry (2014). "Persistence of amygdala gamma oscillations during extinction learning predicts spontaneous fear recovery." Neurobiology of learning and memory **113**: 82-89.

Davis, P., Y. Zaki, J. Maguire and L. G. Reijmers (2017). "Cellular and oscillatory substrates of fear extinction learning." Nature neuroscience **20**(11): 1624-1633.

Dimidschstein, J., Q. Chen, R. Tremblay, S. L. Rogers, G.-A. Saldi, L. Guo, Q. Xu, R. Liu, C. Lu and J. Chu (2016). "A viral strategy for targeting and manipulating interneurons across vertebrate species." Nature neuroscience **19**(12): 1743-1749.

Dong, S., J. A. Allen, M. Farrell and B. L. Roth (2010). "A chemical-genetic approach for precise spatio-temporal control of cellular signaling." Molecular BioSystems **6**(8): 1376-1380.

Douglas Bates, M., B. Bolker and S. Walker (2015). "Fitting linear mixed-effects models using lme4." Journal of Statistical Software **67**(1): 1-48.

Ferretti, V., F. Maltese, G. Contarini, M. Nigro, A. Bonavia, H. Huang, V. Gigliucci, G. Morelli, D. Scheggia, F. Managò, G. Castellani, A. Lefevre, L. Cancedda, B. Chini, V. Grinevich and F. Papaleo (2019). "Oxytocin Signaling in the Central Amygdala Modulates Emotion Discrimination in Mice." Current biology: CB.

Freeman, S. M. and L. J. Young (2016). "Comparative perspectives on oxytocin and vasopressin receptor research in rodents and primates: Translational implications." Journal of Neuroendocrinology.

Freund, T. F. and A. I. Gulyás (1996). "Interneurons of the Hippocampus." Hippocampus **6**(4): 347-470.

Gabbott, P. L., B. G. Dickie, R. R. Vaid, A. J. Headlam and S. J. Bacon (1997). "Local-circuit neurones in the medial prefrontal cortex (areas 25, 32 and 24b) in the rat: morphology and quantitative distribution." Journal of Comparative Neurology **377**(4): 465-499.

Gabbott, P. L., T. A. Warner, P. R. Jays, P. Salway and S. J. Busby (2005). "Prefrontal cortex in the rat: projections to subcortical autonomic, motor, and limbic centers." Journal of Comparative Neurology **492**(2): 145-177.

Gangopadhyay, P., M. Chawla, O. Dal Monte and S. W. Chang (2021). "Prefrontal–amygdala circuits in social decision-making." Nature neuroscience **24**(1): 5-18.

Gifford III, G. W., K. A. MacLean, M. D. Hauser and Y. E. Cohen (2005). "The neurophysiology of functionally meaningful categories: macaque ventrolateral prefrontal cortex plays a critical role in spontaneous categorization of species-specific vocalizations." Journal of cognitive neuroscience **17**(9): 1471-1482.

Grinevich, V., H. S. Knobloch-Bollmann, M. Eliava, M. Busnelli and B. Chini (2016). "Assembling the puzzle: pathways of oxytocin signaling in the brain." Biological psychiatry **79**(3): 155-164.

Grinevich, V. and R. Stoop (2018). "Interplay between oxytocin and sensory systems in the orchestration of socio-emotional behaviors." Neuron **99**(5): 887-904.

Grund, T., Y. Tang, D. Benusiglio, F. Althammer, S. Probst, L. Oppenländer, I. D. Neumann and V. Grinevich (2019). "Chemogenetic activation of oxytocin neurons: Temporal dynamics, hormonal release, and behavioral consequences." Psychoneuroendocrinology **106**: 77-84.

Gur, R., A. Tendler and S. Wagner (2014). "Long-Term Social Recognition Memory Is Mediated by Oxytocin-Dependent Synaptic Plasticity in the Medial Amygdala." Biological psychiatry.

He, Z., L. Young, X.-M. Ma, Q. Guo, L. Wang, Y. Yang, L. Luo, W. Yuan, L. Li, J. Zhang, W. Hou, H. Qiao, R. Jia and F. Tai (2019). "Increased anxiety and decreased sociability induced by paternal deprivation involve the PVN-PrL OTergic pathway." eLife **8**.

Heidbreder, C. A. and H. J. Groenewegen (2003). "The medial prefrontal cortex in the rat: evidence for a dorso-ventral distinction based upon functional and anatomical characteristics." Neuroscience & Biobehavioral Reviews **27**(6): 555-579.

Insel, T. R., B. S. Gingrich and L. J. Young (2001). "Oxytocin: who needs it?" Progress in brain research **133**: 59-66.

Iwasaki, M., A. Lefevre, F. Althammer, E. Clauss Creusot, O. Łąpieś, H. Petitjean, L. Hilfiger, D. Kerspern, M. Melchior and S. Küppers (2023). "An analgesic pathway from parvocellular oxytocin neurons to the periaqueductal gray in rats." Nature Communications **14**(1): 1066.

Jung, K., Y. Choi and H.-B. Kwon (2022). "Cortical control of chandelier cells in neural codes." Frontiers in Cellular Neuroscience **16**: 992409.

Kingsbury, L., S. Huang, J. Wang, K. Gu, P. Golshani, Y. E. Wu and W. Hong (2019). "Correlated neural activity and encoding of behavior across brains of socially interacting animals." Cell **178**(2): 429-446. e416.

Knobloch, H. S., A. Charlet, L. C. Hoffmann, M. Eliava, S. Khrulev, A. H. Cetin, P. Osten, M. K. Schwarz, P. H. Seeburg and R. Stoop (2012). "Evoked axonal oxytocin release in the central amygdala attenuates fear response." Neuron **73**(3): 553-566.

Ko, J. (2017). "Neuroanatomical substrates of rodent social behavior: the medial prefrontal cortex and its projection patterns." Frontiers in neural circuits **11**: 41.

Kolk, S. M. and P. Rakic (2022). "Development of prefrontal cortex." Neuropsychopharmacology **47**(1): 41-57.

Kuznetsova, A., P. B. Brockhoff and R. H. B. Christensen (2017). "lmerTest package: tests in linear mixed effects models." Journal of statistical software **82**(13).

Lee, E., I. Rhim, J. W. Lee, J.-W. Ghim, S. Lee, E. Kim and M. W. Jung (2016). "Enhanced neuronal activity in the medial prefrontal cortex during social approach behavior." Journal of Neuroscience **36**(26): 6926-6936.

Lefevre, A., J. Meza and C. T. Miller (2024). "Long-range projections of oxytocin neurons in the marmoset brain." Journal of Neuroendocrinology **36**(6): e13397.

Lenith, R. (2023). "Estimated Marginal Means, Aka Least-Squares Means." R package Version **1**: 1-1.

Levy, D. R., T. Tamir, M. Kaufman, A. Parabucki, A. Weissbrod, E. Schneidman and O. Yizhar (2019). "Dynamics of social representation in the mouse prefrontal cortex." Nature neuroscience **22**(12): 2013-2022.

Liu, Y., A. Li, C. Bair-Marshall, H. Xu, H. J. Jee, E. Zhu, M. Sun, Q. Zhang, A. Lefevre and Z. S. Chen (2023). "Oxytocin promotes prefrontal population activity via the PVN-PFC pathway to regulate pain." Neuron **111**(11): 1795-1811. e1797.

Mamounas, L. A., C. A. Altar, M. E. Blue, D. R. Kaplan, L. Tessarollo and W. E. Lyons (2000). "BDNF promotes the regenerative sprouting, but not survival, of injured serotonergic axons in the adult rat brain." Journal of Neuroscience **20**(2): 771-782.

Markram, H., J. Lübke, M. Frotscher, A. Roth and B. Sakmann (1997). "Physiology and anatomy of synaptic connections between thick tufted pyramidal neurones in the developing rat neocortex." The Journal of physiology **500**(2): 409-440.

Marlin, B. J. and R. C. Froemke (2016). "Oxytocin modulation of neural circuits for social behavior." Developmental Neurobiology.

Marlin, B. J., M. Mitre, J. A. D'amour, M. V. Chao and R. C. Froemke (2015). "Oxytocin enables maternal behaviour by balancing cortical inhibition." Nature.

Menon, R., T. Grund, I. Zoicas, F. Althammer, D. Fiedler, V. Biermeier, O. J. Bosch, Y. Hiraoka, K. Nishimori and M. Eliava (2018). "Oxytocin signaling in the lateral septum prevents social fear during lactation." Current Biology **28**(7): 1066-1078. e1066.

Meyer-Lindenberg, A., G. Domes, P. Kirsch and M. Heinrichs (2011). "Oxytocin and vasopressin in the human brain: social neuropeptides for translational medicine." Nature Reviews Neuroscience **12**(9): 524-538.

Mohapatra, A. N., S. Netser and S. Wagner (2022). "Modular electrode array for multi-site extracellular recordings from brains of freely moving rodents." Current Protocols **2**(5): e399.

Myers-Schulz, B. and M. Koenigs (2012). "Functional anatomy of ventromedial prefrontal cortex: implications for mood and anxiety disorders." Molecular psychiatry **17**(2): 132-141.

Nakajima, M., A. Görlich and N. Heintz (2014). "Oxytocin Modulates Female Sociosexual Behavior through a Specific Class of Prefrontal Cortical Interneurons." Cell **159**(2): 295-305.

Netser, S., A. Meyer, H. Magalnik, A. Zylbertal, S. H. de la Zerda, M. Briller, A. Bizer, V. Grinevich and S. Wagner (2020). "Distinct dynamics of social motivation drive differential social behavior in laboratory rat and mouse strains." Nature Communications **11**(1): 5908.

Neumann, I. D. and D. A. Slattery (2015). "Oxytocin in General Anxiety and Social Fear: A Translational Approach." Biological Psychiatry.

Newmaster, K. T., Z. T. Nolan, U. Chon, D. J. Vanselow, A. R. Weit, M. Tabbaa, S. Hidema, K. Nishimori, E. A. Hammock and Y. Kim (2020). "Quantitative cellular-resolution map of the oxytocin receptor in postnatally developing mouse brains." Nature communications **11**(1): 1-12.

Ninan, I. (2011). "Oxytocin suppresses basal glutamatergic transmission but facilitates activity-dependent synaptic potentiation in the medial prefrontal cortex." Journal of Neurochemistry **119**(2): 324-331.

Osakada, T., R. Yan, Y. Jiang, D. Wei, R. Tabuchi, B. Dai, X. Wang, G. Zhao, C. X. Wang and J.-J. Liu (2024). "A dedicated hypothalamic oxytocin circuit controls aversive social learning." Nature: 1-10.

Rein, B., K. Ma and Z. Yan (2020). "A standardized social preference protocol for measuring social deficits in mouse models of autism." Nature protocols **15**(10): 3464-3477.

Reppucci, C. J. and G. D. Petrovich (2016). "Organization of connections between the amygdala, medial prefrontal cortex, and lateral hypothalamus: a single and double retrograde tracing study in rats." Brain Structure and Function **221**: 2937-2962.

Rogers, C. N., A. P. Ross, S. P. Sahu, E. R. Siegel, J. M. Dooyema, M. A. Cree, E. G. Stopa, L. J. Young, J. K. Rilling and H. E. Albers (2018). "Oxytocin-and arginine vasopressin-containing fibers in the cortex of humans, chimpanzees, and rhesus macaques." American journal of primatology **80**(10): e22875.

Russell, J. A., G. Leng and A. J. Douglas (2003). "The magnocellular oxytocin system, the fount of maternity: adaptations in pregnancy." Frontiers in neuroendocrinology **24**(1): 27-61.

Saunders, A., C. A. Johnson and B. L. Sabatini (2012). "Novel recombinant adeno-associated viruses for Cre activated and inactivated transgene expression in neurons." Frontiers in neural circuits **6**: 47.

Schiavo, J. K., S. Valtcheva, C. J. Bair-Marshall, S. C. Song, K. A. Martin and R. C. Froemke (2020). "Innate and plastic mechanisms for maternal behaviour in auditory cortex." Nature **587**(7834): 426-431.

Schneider, C. A., W. S. Rasband and K. W. Eliceiri (2012). "NIH Image to ImageJ: 25 years of image analysis." Nature methods **9**(7): 671-675.

Schuster, R., B. D. Berger and H. H. Swanson (1988). "Cooperative social coordination and aggression: sex and strain differences in the effects of housing on gonadectomized rats with hormone replacement." Aggressive Behavior **14**(4): 275-290.

Somogyi, P. (1977). "A specific 'axo-axonal'interneuron in the visual cortex of the rat." Brain Res **136**(2): 345-350.

Stuart, G., H. Dodt and B. Sakmann (1993). "Patch-clamp recordings from the soma and dendrites of neurons in brain slices using infrared video microscopy." Pflügers Archiv **423**: 511-518.

Swanson, L. W. and P. E. Sawchenko (1983). "Hypothalamic Integration: Organization of the Paraventricular and Supraoptic Nuclei." Annual Review of Neuroscience **6**(1): 269-324.

Szlaga, A., P. Sambak, A. Trenk, A. Gugula, C. Singleton, G. Drwiega, T. Blasiak, S. Ma, A. Gundlach and A. Blasiak (2022). Functional neuroanatomy of the rat nucleus incertus-medial septum tract: implications for the cell-specific control of the septohippocampal pathway. Front Cell Neurosci 16: 836116.

Tan, Y., S. M. Singhal, S. W. Harden, K. M. Cahill, D.-T. M. Nguyen, L. M. Colon-Perez, T. J. Sahagian, J. S. Thinschmidt, A. D. de Kloet, M. Febo, C. J. Frazier and E. G. Krause (2019). "Oxytocin receptors are expressed by glutamatergic prefrontal cortical neurons that selectively modulate social recognition." The Journal of Neuroscience: The Official Journal of the Society for Neuroscience.

Tang, Y., D. Benusiglio, A. Lefevre, L. Hilfiger, F. Althammer, A. Bludau, D. Hagiwara, A. Baudon, P. Darbon and J. Schimmer (2020). "Social touch promotes interfemale communication via activation of parvocellular oxytocin neurons." Nature Neuroscience **23**(9): 1125-1137.

Valtcheva, S. and R. C. Froemke (2018). "Neuromodulation of maternal circuits by oxytocin." Cell and Tissue Research.

Veenema, A. H. and I. D. Neumann (2008). "Central vasopressin and oxytocin release: regulation of complex social behaviours." Progress in brain research **170**: 261-276.

Yang, S.-S., N. R. Mack, Y. Shu and W.-J. Gao (2021). "Prefrontal GABAergic interneurons gate long-range afferents to regulate prefrontal cortex-associated complex behaviors." Frontiers in neural circuits **15**: 716408.

Young, L. J. (1999). "Oxytocin and vasopressin receptors and species-typical social behaviors." Hormones and Behavior **36**(3): 212-221.

METHODS

Animals

We obtained female Sprague-Dawley rats aged between 3 and 8 weeks from Janvier Labs, and all animals from the transgenic OTR-Cre rat line were bred in the breeding facility at the Central Institute for Mental Health in Mannheim, Germany. We ensured their accommodation in standard lab settings, including a consistent 12-hour light-dark cycle with illumination beginning at 07:00, ambient temperatures maintained at 22–24 °C, and relative humidity kept around 50 ± 5%. Animals were group-housed in conventional EU Makrolon type IV cages and had unrestricted access to both food and water unless stated differently in the experimental procedure. The research procedures conducted in the laboratory of VG adhered to the legal requirements set by German legislation and were approved under license number G-193/20 and G-55/23 by the Baden Württemberg's German Animal Ethics Committee. In vivo electrophysiological experiments were conducted in the laboratory of SW according to the National Institutes of Health guide for the care and use of laboratory animals and approved by the Institutional Animal Care and Use Committee (IACUC) of the University of Haifa (Ethical License number UoH - IL - 2307 - 132 – 4).

OTR -Cre rats

Transgenic OTR-Cre rats (Iwasaki, Lefevre et al. 2023) express Cre recombinase in all OTR neurons, therefore allowing the specific expression of Cre-dependent (DIO – double floxed inverted orientation) AAVs. Animals were bred within the institute as the offspring of WT female rats and heterozygous Cre+ male rats. The offsprings were either heterozygous Cre+ or Cre- animals and were therefore genotyped utilizing a PCR-based approach.

Viruses

In the current study, recombinant adeno-associated viruses (rAAVs) of serotype 1/2 were employed, replicating previously established methodologies (Knobloch, Charlet et al. 2012). The HEK293T cells utilized for viral production were sourced from Addgene (catalog number 240073). The OT-promoter controlled rAAV-OTp-ChR2-mCherry as well as floxed rAAVs for the Cre-dependent expression were produced in house: rAAV-Ef1a-DIO-GFP, rAAV-Ef1a-DIO-GCaMP6s, rAAV-Ef1a-DIO-ChR2-mCherry (rAAV titers were between 10^9 and 10^{10} genomic copies/µl). The rAAVs for specific targeting of interneurons were purchased from ETH Zurich viral vector facility (https://vvf.ethz.ch) and were of serotype DJ: rAAV-DLX-DIO-GFP, rAAV-DLX-DIO-mCherry, rAAV-DLX-DIO-Gq-GFP, rAAV-DLX-DIO-Gi-GFP, rAAV-DLX-DIO-ChR2-mCherry (rAAV titers were between 6.5×10^{12} and 8×10^{12} vg/ml). The rAAV system used for knocking out OTRs were serotype 9 and acquired in collaboration with Larry Young and Arjen Boender: rAAV-hSyn-spCas9, rAAV-u6-gRNA(OTR)-hSyn-mCherry, rAAV-u6-gRNA(lacZ)-hSyn-mCherry (rAAV titers were 3.0×10^{10} and 1.5×10^{10} genomic copies/µl for gRNA and Cas9 AAVs, respectively). Retrograde rAAVs were obtained from addgene: retro-rAAV-hSyn-GFP (titer $\geq 7 \times 10^{12}$ vg/mL).

Specific expression in OT neurons

The OT-promoter (OTp) expressed by our rAAVs was used to achieve cell-type specificity in OT neurons (Knobloch, Charlet et al. 2012).

Specific expression in OTR neurons

The Cre-Lox system was used to specifically target OTR neurons in the brains of transgenic rats. The transgenic OTR-Cre rats described above express the Cre-recombinase in all OTR neurons. The inverted gene is only transcribed in the cells which express Cre-recombinase, as it excises and inverts the DIO sequence, thereby enabling its expression (Saunders, Johnson and Sabatini 2012). Thus, only Cre-positive neurons (OTR neurons) are labelled selectively.

Specific expression in OTR interneurons

Specific labelling of OTR interneurons was achieved by combining the Cre-Lox system in transgenic OTR-Cre rats, paired with transcriptional control of the murine distal-less homeobox (mDlx) enhancer element and the human beta-Globin (HBB) minimal promoter fragment, which leads to specific expression restricted to GABAergic interneurons (Dimidschstein, Chen et al. 2016).

Optogenetic AAVs

rAAVs expressing Channelrhodopsin in either OT neurons or OTR neurons was utilized both *in vivo* and *ex vivo*. For *in vivo* experiments, blue light (BL) for the activation of neurons was administered via the implantation of an optic fiber.

Calcium sensor

To record neuronal activity in OTR neurons we utilized a rAAV expressing a calcium sensor (GCaMP6s) in a Cre-dependent manner. Binding of calcium as a proxy for neuronal activity increases fluorescence which is recorded with implanted optic fibers.

Chemogenetic AAVs

The activity of the OTergic system was manipulated by injecting a rAAV carrying excitatory (hM3Dq) or inhibitory (hM4Di) DREADDs (Designer Receptors Exclusively Activated by Designer Drugs) as described in Grund, Tang et al. (2019). Gq-DREADDS increase neuronal activity by signaling through the Gαq/11 G-protein and stimulating phospholipase C, which leads to the release of calcium from intracellular stores. While the genetically introduced DREADDs are integrated into the cell-membrane of injected neurons, they are inactive and have to be activated by i.p. administration of the ligand Clozapine N-oxide (CNO) (Dong, Allen et al. 2010).

OTR knockout AAVs

A viral functional knockout of OTRs was achieved with a novel CRISPR/Cas9 based method previously published by Boender, Boon et al. (2023) consisting of a mixture of one rAAV expressing Cas9 and a second rAAV expressing the guide RNA specific for OTRs.

Stereotactic injections of viral vectors

Rats were initially anesthetized using either isoflurane inhalation (1L/min flow of 4% isoflurane) or injection of ketamine (75 mg/kg of body weight) and xylazine (5 mg/kg of body weight). For the injections, 300 nl of the solution (determined rAAV titers ranged from 10^9 to 10^{10} genomic copies per microliter) was administered per hemisphere in the required brain regions. The viral vectors were delivered into designated brain regions at a rate of 150 nl per minute through a glass micropipette, replicating our methodology from prior studies. The stereotactic coordinates were aligned with established rat brain atlas benchmarks: for PVN (A/P: −1.8 mm, M/L: ±0.3 mm, D/V: −8 mm), SON (A/P: −1.8 mm, M/L: ±1.2 mm, D/V: −9.25 mm), ILC (A/P: 3 mm, M/L: ±0.5 mm, D/V: −4.6 mm), BLA (A/P: −3

mm, M/L: ±5 mm, D/V: −9/-8.4 mm), and NAc (A/P: 1.2 mm, M/L: ±1 mm, D/V: −8.2/-7.8 mm),. After completion of all experiments, validation of the correct injection sites and gene expression was confirmed by histological analysis.

Optogenetic stimulation of OT fibers

For the in vivo optogenetic experiments, rats were injected bilaterally in their hypothalamic nuclei (SON, PV, AN, see above for coordinates) with rAAVs (either rAAV-OTp-Venus or rAAV-OTp-ChR2-mcherry) and optic fibers were implanted bilaterally above the ILC. For the implantation of optic fibers within the ILC the following coordinates were used (M/L ±1.52 mm, A/P +3.1, D/V -4.75, angled at 10°, this angle was essential to allow enough space for connecting the laser patch cables to the implanted optic fibers). The optic fibers were purchased from Thorlabs (Cat.number: CFMC12L10, Fiber Optic Cannula, Ø2.5 mm Ceramic Ferrule, Ø200 µm Core, 0.39 NA, L=10 mm) which were cut at a desired length of 5.5mm by using a fiber scribe (Thorlabs: S90R Ruby DualScribe™ Fiber Optic Scribe) and a digital Vernier dual Caliper meter. Two blue lasers (λ=473nm, output of 100 mW/mm^2, DreamLasers, Shanghai, China) coupled with optical fiber patch cables (Thorlabs; cat.no RJPFF2-FC/PC to Ø2.5 mm Ferrule Rotary Joint Patch Cable, Ø200 µm Core, 3 m Long) were used for optogenetic photostimulation. These fiber patch cables (RJPFF2, Throlabs) were connected to the implantable fibers using a quick-release interconnect mating sleeve (Thorlabs; Cat.no: ADAF2 - Quick-Release Interconnect for Ø2.5 mm Ferrules). BL stimulation was applied (as previously described in Knobloch, Charlet et al. (2012)) at a light intensity of 10 mW/mm^2, 30 Hz, 10 ms pulses, for a duration of 120s. Laser output was controlled using a pulse generator (Master-8), which delivered the 10-ms light pulses at 30 Hz. Light output through the optical fibers was adjusted to 10 mW/mm using a digital power-meter console.

***Ex vivo* electrophysiology**

Slice preparation

Approximately 3 to 6 weeks following the administration of viral vectors brain slices for *ex vivo* patch clamp recordings were prepared. The exact procedures differ depending on specific experiments: (1) TGOT application in current clamp (2) TGOT application in voltage clamp (3) paired patch recordings (4) optogenetic stimulation of OTR+ neurons with recoding of OTR- pyramids (5) optogenetic stimulation of OTR+ interneurons and recording of BLA-projecting pyramids. For experiments 1-4 preparation and visualization of neurons both in living slices and after labeling with biocytin are described elsewhere (Stuart, Dodt and Sakmann 1993, Markram, Lübke et al. 1997). For experiment 5 the following protocol was used.

Rats were anesthetized with isoflurane and decapitated. Brains were removed in chilled carbogenated artificial cerebrospinal fluid (ACSF), containing (in mM): 92 choline chloride, 2.1 KCl, 1.2 NaH_2PO_4, 30 $NaHCO_3$, 20 HEPES, 25 glucose, 5 Na-ascorbate, 2 thiourea, 3 Na-pyruvate, 5 N-acetyl-L-cysteine, 10 $MgSO_4$, 0.5 $CaCl_2$, pH 7.3–7.4; osmolality 290–310 mOsm kg^{-1}; and cut in the same solution into 400 µm thick coronal sections containing vmPFC using a Leica VT 1200 vibrating microtome (Leica Instruments, Heidelberg, Germany). Sections were then incubated for 10 minutes at 32°C in the same carbogenated ACSF and afterwards transferred to carbogenated ACSF containing (in mM): 92 NaCl, 2.1 KCl, 1.2 NaH_2PO_4, 30 $NaHCO_3$, 20 HEPES, 10 glucose, 5 Na-ascorbate, 2 thiourea, 3 Na-pyruvate,

5 N-acetyl-L-cysteine, 1.3 $MgSO_4$, 2.4 $CaCl_2$, pH 7.3–7.4; osmolality 290–310 mOsm kg^{-1} for at least an hour before the recording.

After recording, slices were fixed overnight with 4% formaldehyde in PBS solution at 4°C and immunostained to examine the neurochemical content of recorded neurons. Briefly, free-floating sections were incubated with a primary antibody solution (chicken anti-GFP (1:10000), Streptavidin-iFluor750 (1:4000), rabbit anti-RFP (1:2000), 0.5% Triton X-100 in PBS) for 72 h at 4°C, followed by incubation with a secondary antibody mixture (donkey anti-chicken Alexa Fluor 488-conjugated $F(ab')_2$ Fragment Antibody (1:2000), donkey anti-rabbit Cy3-conjugated $F(ab')_2$ Fragment Antibody (1:2000), 0.5% Tx100 in PBS) for 24 h at 4°C. Each step was followed by multiple PBS washes. Stained sections were mounted and coverslipped with Mowiol mounting medium and imaged with a slide scanner (VS200, Olympus) and a confocal microscope (STELLARIS 5, Leica Microsystems).

Patch-clamp recording

Sections containing vmPFC were transferred to a recording chamber placed on a fixed microscope stage equipped with video-enhanced infrared differential interference contrast (Eclipse FN1, Nikon Europe B.V., Amstelveen, Netherlands). Tissue was perfused (2 ml min^{-1}) with warm (32°C) carbogenated ACSF containing (in mM): for experiments 1-4: 125 NaCl, 25 $NaHCO_3$, 2.5 KCl, 1.25 NaH_2PO_4, 2 $CaCl_2$, and 1 $MgCl_2$ and 25 glucose (pH 7.2, osmolality 290–300 mOsm kg^{-1}) or for experiment 5: 118 NaCl, 25 $NaHCO_3$, 3 KCl, 1.2 NaH_2PO4, 2 $CaCl_2$, 1.3 $MgSO_4$, and 10 glucose, (pH 7.4, osmolality 290–300 mOsm kg^{-1}).

Recording micropipettes fabricated from borosilicate glass capillaries (5–7 MΩ) using a horizontal puller (Sutter Instruments) were filled with a solution containing following solutions (in mM): for experiment 1 and 4: 144 K gluconate, 4 KCl, 4 Mg-ATP, 10 phosphocreatine, 0.3 GTP, and 10 HEPES (pH 7.3, KOH, 293 mOsm); for experiment 2: 144 Cs gluconate, 4 CsCl, 4 Mg-ATP, 10 phosphocreatine, 0.3 GTP, and 10 HEPES (pH 7.3, CsOH, 293 mOsm); for experiment 3: 110 K gluconate, 30 KCl, 8 NaCl, 4 Mg-ATP, 10 phosphocreatine, 0.3 GTP, and 10 HEPES (pH 7.3, KOH, 293 mOsm); for experiment 5: 145 K gluconate, 2 $MgCl_2$, 4 Na_2ATP, 0.4 Na_3GTP, 5 EGTA, 10 HEPES, (pH 7.3, KOH, 290-300 mOsm kg^{-1}) and biocytin (0.05% w/v) for subsequent immunofluorescent identification of recorded neurons.

Whole-cell configurations were obtained using negative pressure applied by mouth suction. EPC 10 USB double amplifier and Patchmaster software (HEKA, Multi Channel Systems MCS GmbH, Reutlingen, Germany) were used for signal recording and data acquisition. Recorded signals were low-pass filtered at 2.9 kHz and digitized at 50 kHz. Neurons were identified by fluorescent marker expression, cell body appearance, location in the slice, firing pattern and post-recording staining.

In experiment 3 presynaptic cells were stimulated with a 10 Hz train of 3 suprathreshold current pulses. Trains were delivered at intervals of 7 s. Voltage traces shown are averages of 50–100 sweeps. The success rate of finding a synaptic coupling was calculated as the inverse (in %) of the number of neurons tested before a connection was found. In experiment 2, spontaneous EPSCs and IPSC were recorded at -90 mV (E_{AMPA}) and 0 mV (E_{GABA}), respectively. In experiment 5 only cells classified as ILC layer 2/3 pyramidal neurons innervating BLA were included in the analysis. Cells were voltage-clamped at -60 mV and subjected to a 10 ms BL pulse (~10 mW) every 30 seconds for a total of 10 pulses. The resulting traces were then averaged.

Data analysis

Analyses were performed using IGOR PRO software (Wavemetrics, Lake Oswego, OR), Signal software (CED, Cambridge, UK) and MATLAB. Electrophysiological data in the graphs and text are given as the mean ± SD. Calculation of the statistical significance of differences was performed using unpaired, two-tailed Student's t test. The significance of statistical differences in the analysis of cumulative histograms was assessed using the Smirnov-Kolmogorov test.

In experiment 2 postsynaptic currents were detected using a deconvolution algorithm in a custom-written MATLAB routine. Briefly, data sampled at 10000/s was low-pass filtered at 200 Hz and then deconvolved by the Wiener filter (MATLAB-intrinsic deconvwnr function) with a point-spread-function using the following parameters for tau_onset and tau_offset: 4 ms and 15 ms for IPSCs and 2.5 ms and 10 ms for EPSCs, respectively. In the deconvolved trace, PSC peaks were detected as local maxima in a 50 ms sliding window using a 2-step dynamic and absolute threshold. PSC features were then extracted from traces around the peaks.

***In vivo* electrophysiology (MEA)**

Surgery for electrode array implantation

Three weeks after the viral injection surgery, the rats were anesthetized by intraperitoneal injection of ketamine and Domitor (0.09 mg/gr and 0.0055 mg/gr, respectively). Toe-pinch reflexes were monitored to test the level of anesthesia. Rats were fixed in a stereotaxic apparatus (Stoelting Inst.). The anesthetized state of the rats was maintained for the whole surgery (3-4 hours) with isoflurane through a low-flow anesthesia system (0.5–1%, 200 mL/min; SomnoFlo, Kent Scientific). The animal was placed on a heating pad connected to a closed-loop custom-made temperature controller to maintain the body temperature at 37°C. Two holes were drilled on the skull to place the reference and ground wires (silver wire, 127 µm, 200-500 Ω; A-M Systems, Carlsborg, WA). A custom-made multi-electrode array (MEA) was prepared as explained in Mohapatra, Netser and Wagner (2022) to target the ILC (AP = 1 mm, ML = −0.3 mm, DV = −4.28 mm) and BLA (AP = -4 mm, ML = −4.6 mm, DV = −8.6 mm). Each of these brain areas was targeted with three adjacent electrodes, of which one was selected for analysis of electrical signals (see below). The electrodes in the MEA were coated in DiI (1,1'-Dioctadecyl3,3,3',3'-tetramethylindocarbocyanine perchlorate; 42364, SigmaAldrich) to trace their location post-mortem. Two watch screws (0-80, 1/16", M1.4) were inserted into the temporal bone for structural support. The surface of the brain was exposed by removing the skull covering the mentioned brain areas. The MEA was inserted slowly into the brain manually with the help of the stereotaxic apparatus. The MEA and screws were secured with dental cement (Enamel plus, Micerium). Following surgery, rats received daily injections of meloxicam (1 mg/kg) and amoxycillin (0.07mg/gr) for three days and were allowed to recover for at least 7 days with other implanted cagemates before experiments.

Electrophysiological and video recording setup

Following a brief exposure to isoflurane, subjects were attached to a headstage board (RHD 16 ch, #C3334, Intan Technologies) through a custom-made Omnetics to Mill-Max adaptor (Mill-Max model 852-10-100-10-001000). Behavior was recorded above the arena using a monochromatic camera (30 Hz, Flea3 USB3, Flir). Electrophysiological recordings were made with the RHD2000 evaluation system using an ultra-thin SPI interface cable connected to the headstage board. Electrophysiological

recordings (sampled at 20 kHz) were aligned with recorded video using a TTL trigger pulse and by recording camera frame strobes.

Electrophysiological recordings

Each recording session was divided into two 5 min stages, namely, a baseline period during which time the subject was alone in the arena in the presence of two empty chambers and a task (encounter) period when the subject performed the task. Each subject was evaluated over two sessions of the social vs. food task, one with saline injection and one with CNO injection (3mg/kg), administered 40 min before the session.

Histology

Subjects were trans-cardially perfused, and their brains were kept cold in 4% paraformaldehyde in PBS for 48 hours. Brains were washed carefully in PBS, sectioned (50 µm) in the horizontal plane with a vibrating blade microtome (VT 1200s, Leica) and collected onto microscope slides. Electrode marks were visualized (DiI coated, Red) against DAPI-stained sections with an epifluorescence microscope (Ti2 eclipse, Nikon).

Electrophysiological data analysis

Following the histological examination, we selected the electrode located at the center of the desired brain structure for analysis of electrophysiological signals. All signals were analyzed using custom-made codes written in MATLAB 2020a. We excluded signals recorded during 30 seconds around stimulus removal and insertion times to avoid any artifacts due to these actions. The signals were first down-sampled to 5 kHz and low-pass filtered to 300 Hz using a Butterworth filter. The power and time for the different frequencies were estimated using the 'spectrogram' function in MATLAB with the following parameters: Discrete prolate spheroidal sequences (dpss) window = 2 s; overlap = 50%; increments = 0.5 Hz; and time bins = 0.5 s. The power of each frequency band (theta: 4-12 Hz and gamma: 30-80 Hz) was averaged for both the baseline and encounter periods (5 min each). Changes in theta and gamma power for each brain region were defined as the mean difference in power between the encounter and baseline periods.

In vivo fiber photometry

Implantation of optic fibers

We injected a modified adenovirus (AAV-Ef1a-DIO-GCaMP6s) bilaterally into the vmPFC (450 nL, A/P: 3.1mm, M/L: +-1.52 mm, D/V: -5 mm, angle 10°) of OTR-Cre positive female rats (n=4) to transduce expression of the Ca^{2+} indicator, GCaMP6s, in oxytocin receptor/Cre expressing neurons. During the same surgery, optic fibers (Ø 400µm, 0.50 NA, 5.5 mm, Thorlabs) were implanted ~100 µm above the ILC (A/P: 3.1mm, M/L: +-1.52 mm, D/V: -4.9 mm, angle 10°). Four 1 mm screws (Knupfer,1042 Germany) were attached to skull with and fixed with dental cement (Paladur, Heraeus Kulzer, Germany). Throughout this procedure, rats were under 1.5% isoflurane anesthesia and body temperature was kept stable at 37° C by a heating plate (RWD,1054 China). Animals were monitored post-op and administered carprofen for 3 days.

Fiber photometry data acquisition

Rats (n=4) were recorded for 10 minutes in a square open field arena. After the first 5 minutes alone to allow habituation to the environment, an unknown female rat or a toy was introduced. Behavior events (anogenital sniffing, non-anogenital sniffing, and toy sniffing) performed by both the test and stimulus rat were manually scored using BORIS video analysis software (https://www.boris.unito.it/). Furthermore, behaviors were categorized as either active social behavior (test rat investigating the stimulus rat), or received social behavior (stimulus rat investigating test rat). Each rat underwent multiple sessions (total: 44 recordings across 4 rats). Data were acquired using a Doric fiber photometry system and Doric Neuroscience Studio v6.1 software (Doric Lenses, Quebec, Canada) with 0.4mW of LED power output at the tip of the optic fiber, a 20 Hz acquisition frequency (10 ms light pulses) at 470nm for the calcium signal and 405nm for the isosbestic signal. The system was connected to the rat through 2 x 1m long optic fiber cables interfaced with a double rotary joint. Videos were recorded using the same hardware/software interface to allow for precise temporal synchronization of the behaviors and recorded signals.

Fiber photometry data analysis

Raw data was extracted through Doric Neuroscience Studio v6.1 and preprocessed (smoothing to remove high frequency noise, Δ F/F was calculated as (calcium signal – scaled isosbestic signal)/scaled isosbestic signal, and subsequently Z scored), using pMat toolbox (Bruno, O'Brien et al. 2021). We compared the normalized signal averaged over 1 second before the onset of a behavioral event (anogenital sniffing, non-anogenital sniffing, toy sniffing) to the normalized signal averaged over the first second after the onset of the behavioral event.

Statistical linear mixed effect model

Statistical analysis was performed in R (Version 4.0.4; Team RC, 2021. https://www.R-project.org/) and RStudio (Version 1.4.1106, PBC; Team R, 2019. http://www.rstudio.com/). Linear mixed-effects models were fitted with *lme4* (Douglas Bates, Bolker and Walker 2015) and *lmerTest* (Kuznetsova, Brockhoff and Christensen 2017) packages and analyzed with type III ANOVA (Satterthwaite's method). *Post hoc* analyses (Tukey's multiple comparison) were performed using the *emmeans* package (Lenith 2023), together with the Kenward–Roger approximation for denominator degrees of freedom. Assumptions for using a linear model were checked by residual plot inspection.

Two linear mixed effects models were fitted. The first one compared the z-scored recorded signal just before and during each behavioral event in a paired manner by adding trial as a random effect. Trial was nested within a recording, as each animal underwent multiple recording sessions. Since most of the optic probes were almost always present in both hemispheres, we also nested a recording (from each side) within session. Lastly, sessions were nested within animal. Overall, the random effect consisted of trial number within recording within session within animal. Fixed factors included time in relation to trial onset (before vs during the behavior) and behavior (anogenital, non-anogenital, toy) in order to determine if any of the behaviors caused significant changes in the recorded signal while they were performed.

The second model was fitted to analyze differences between types of behavior (active social, received social) by comparing the amplitudes of signal change (subtracted values before from during). This

model consisted of behavior type as a fixed factor and the same random effect structure as the previous model, without the trial factor.

Behavior tests

Adult female rats (8-12 weeks) were used for all behavioral tests. The rats were tested for their estrous cycle and only animals in diestrus phase of the cycle were included in experiments in analogy to Tang, Benusiglio et al. (2020). Behavioral assessments took place in a specially designed odor-resistant arena measuring 60 cm in length, width, and height, under low-intensity lighting conditions (<20 lux, as measured by a SO 200K lux-meter from Sauter). To acclimatize the rats to the test environment, each subject was allowed a 15-minute habituation session in the arena the day before actual testing. After each use, the arena was thoroughly sanitized with 80% ethanol to remove any odors of previous tests. To prevent any bias from prior interactions, the experimental rats and the stimulus rats (used as social stimuli during tests) were housed separately and had no previous encounters with one another. This approach ensured that all social interactions during the tests were with novel, unfamiliar conspecifics, maintaining the integrity and consistency of the experimental conditions.

Free social interaction

Animals interacted with unknown conspecifics for 5 minutes in the open field arena. The stimulus rats were matched with the experimental rats in regards to strain, age (same age or up to one week younger), sex, and weight (within ± 10 g). Both the experimental rats and the stimulus counterparts were simultaneously introduced into diagonally opposite corners of the testing arena. This arrangement permitted the animals to engage naturally with one another or to independently explore their surroundings. For optogenetic manipulation, BL was activated (light intensity of 10 mW/mm^2, 30 Hz, 10 ms pulses) during the first two minutes of the session. For chemogenetic activation, the DREAAD-agonist CNO was injected 40 min prior to the interaction (3mg/kg). All behaviors (anogenital- and non-anogenital-sniffing, following and approaching, and toy investigation behavior were manually scored using the BORIS video analysis software (https://www.boris.unito.it).

Food vs Social preference test

The experiment was performed in the same square arena, with the addition of two triangular dividers in opposite corners with a front mesh. The mesh allowed for indirect interaction with an unknown social partner (only sniffing or hearing) but no direct social touch, or investigation of food pellets (only sniffing) without eating them. Test sessions lasted 5 minutes (after 15 minutes of habituation on each day), where the rat could freely investigate the two corners with either an unknown female rat (3-4 weeks) or standard food pellets. On the next day, after 24h of food deprivation, the test was repeated. Investigation time of both corner zones was analysed using the Ethovision XT v.11.5 (Noldus) software.

The social preference index was calculated as described in the literature (Rein, Ma and Yan 2020):

$$SPI = \frac{social\ corner\ (s)\ -\ food\ corner\ (s)}{social\ corner(s)\ +\ food\ corner\ (s)}$$

with a positive SPI indicating a preference for the social corner, and a negative SPI indicating a preference for the food corner.

Histology

Rats under anesthesia underwent trans-cardial perfusion, initially with phosphate-buffered saline (PBS) and subsequently with 4% paraformaldehyde (PFA). The brains were then extracted from the cranium and immersed in 4% PFA for an overnight post-fixation at 4°C. Coronal sections of 50 µm thickness were obtained using a vibratome (Leica-VT 1000S) and collected into series, representing the rostro-caudal aspects of the hypothalamic OT system and the ILC, respectively. The immunohistochemical labelling was conducted in accordance to well-established and widely-used protocols. We applied highly specific antibodies: anti-OT (PS38, 1:2,000; mouse; kindly provided by H. Gainer), anti-Ds-Red (Clontech, catalog no. 632397, 1:1,000; rabbit), anti-GFP (Abcam, ab13970, 1:1,000, chicken), anti-cFos (Cell Signaling, catalog no. 9F6, 1:500, rabbit), anti-NeuN (Merck, MAB377, 1:1000, mouse), anti-Ankyrin (Millipore, MABN466, 1:1000, mouse). The target antigens were visualized with the following conventional secondary antibodies: CysTyr3 conjugate (711-165-152) or CysTyr5 conjugate (Jackson Immuno-Research Laboratories, 115-175-146) or Alexa 488 (Invitrogen, A11039) and Alexa 594 (Invitrogen, A11012) and Alexa-594 (Jackson Immuno-Research Laboratories, 715- 585-151) and Alexa-647 (Jackson Immuno-Research Laboratories, 713-645-147). All secondary antibodies were diluted 1:1000.

Microscopy

Large scale automated scanning of labelled brain sections was conducted with the slide-scanner (Olympus SLIDEVIEW VS200) microscope, which allowed to obtain high-resolution over-views of the entire areas of interest and the virus injection sites in whole brain sections. For the documentation/imaging of individual neuron morphologies, co-expression of reported cell markers as well as proximity of OT fibers to their mutual target neurons in the ILC, we employed confocal laser scanning microscopy (CLSM Leica Stellaris 5) in the Z-stack mode.

Fiber quantification analysis

Densities of OT-positive fibers were quantified in serial sections collected between Bregma 3.72 and Bregma 2.52 corresponding to the rostral and caudal borders of the ILC (n = 11 sections from 3 animals). The anatomical borders between the mPFC subdivisions were defined based on Paxinos Rat Brain Atlas and previous cytoarchitectonic studies (Kolk and Rakic 2022). The whole-brain section scans of the planes containing Cg1, PrL and ILC were captured with an Olympus VS200 slide-scanning microscope at 20x magnification and then stitched into VSI image files. Fiber densities were quantified by counting crossing points of OT fibers in digitalized images overlayed with a non-destructive grid of lines (Mamounas, Altar et al. 2000) in ImageJ. Numbers of crossing points within Cg1, PrL and ILC were averaged for all images taken from an individual animal. The densities of OT fibers between the three mPFC subdivisions were compared using a one-way ANOVA. p-values < 0.05 were deemed to be significant.

Neuron quantification analysis

For each animal, one of four series of 50µm sections through the rostral to caudal aspect of the ILC was analyzed to describe the relative quantification of OTR-expressing cells. This analysis was performed for 1) the proportion of inhibitory vs. excitatory OTR-expressing neurons in the entire ILC, and for 2) quantification of co-expression of cytochemical markers of OTR-expressing ILC neurons.

Therefore, we manually counted the OTR-GFP expressing neurons vs. appropriate neuronal cell markers in ImageJ, applying the touch-count mode. Counted neurons of interest were averaged and presented as the percent fraction of the total OTR-expressing neurons.

Automated image analysis and cFos quantification via Imaris

After immunohistochemical staining against GFP, cFos and NeuN, images containing brain regions of interest were acquired using the Olympus Slideview VS200 slide scanner at 20x magnification. Image files were then converted into TIFF files using Qupath and imported into Imaris 10.0 (Oxford Instruments). Next, the spot function was used to identify both NeuN-positive cells and cFos expression in specifically defined regions of interest such as the mPFC, NAc or BLA. Excel files containing information about total neuronal numbers, total cFos signal and NeuN/cFos overlap was exported and compiled for further statistical analysis.

Western blot

Protein from the brains of OTR-Cre and WT-rats was extracted using RIPA Lysis buffer and concentration was measured using a BCA-kit according to the manufacturer's instructions. The protein samples were separated by molecular weight using a 4-12% NuPage Bis-Tris-Gel (Invitrogen, Thermo Fisher Scientifics, USA) and NuPage MES-Buffer (Invitrogen, Thermo Fisher Scientifics, USA). The gel was blotted on nitrocellulose-membrane and blocked in 5% milk in TBS-T. The membrane was incubated overnight with primary antibodies rabbit anti-oxytocin-receptor (Thermo Fisher Scientifics; dilution:1:1000) and mouse anti-GAPDH (abcam; dilution 1:5000). For visualization, the membrane was incubated with secondary antibodies HRP-anti-rabbit and HRP-anti-mouse and chemiluminescence was performed. Bands were then quantified using ImageJ.

Multiplex fluorescent in situ hybridization

To characterize the expression profile of OTR neurons in the ILC, we performed in situ hybridization using the RNAscope™ HiPlex Assay (Advanced Cell Diagnostics, Hayward, CA, USA) for AF488, Atto550, and Atto647 detection. All procedures were conducted using fresh frozen 16 µm brain sections (2 ILC-containing slices per brain, 2 female rat brains), adhering to the manual and as previously described (Szlaga, Sambak et al. 2022). During the initial hybridization steps, the following probes were applied: vGlut1 (Rn-Slc17a7-T1, cat. no. 317001-T1, ACD); Cre (CRE-T2, cat. no. 312281-T2, ACD); vGAT1 (Rn-Slc32a1-T3, cat. no. 424541-T3, ACD); vGlut2 (Rn-Slc17a6-T5, cat. no. 31701-T5, ACD); and OTR (Rn-Oxtr-T6, cat. no. 483671-T6, ACD). Images were acquired using an Axio Imager M2 fluorescent microscope (Zeiss, Gottingen, Germany) with an automatic z-stage and Axiocam 503 mono camera (Zeiss). Zen (3.1 blue edition and 3.0 SR black edition, Zeiss), CorelDraw 2020 (Corel Corporation, Ottawa, Canada), ImageJ (Schneider, Rasband and Eliceiri 2012), and HiPlex Image Registration Software v1.0 (ACD) were employed for image processing. OTR mRNA-expressing cells in the ILC region from one brain hemisphere per section were investigated for colocalization with Cre, vGAT1, vGlut1, and vGlut2 mRNAs. Neurons were identified by the presence of a DAPI-stained nucleus and/or an unambiguous cell-like distribution of fluorescent mRNA dots, and counted using the ImageJ Cell Counter plugin (Schneider, Rasband and Eliceiri 2012) in analogy to Iwasaki, Lefevre et al. (2023).

EXTENDED DATA

Figure S1

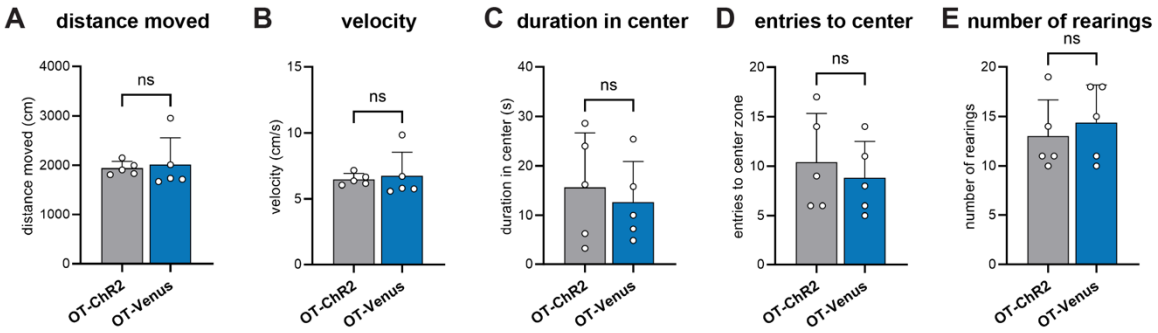

Extended Data Figure 1.
A Distance moved and **B** velocity in the open field, a control for locomotor effects, remain unchanged by optogenetic manipulation of OT axons in the ILC. **C** Duration in center and **D** entries to center, a control for anxiety-like behavior, remain unchanged by optogenetic manipulation. **E** Number of rearings as a non-social behavior is not affected by optogenetic manipulation (n=5 animals per group).

Figure S2

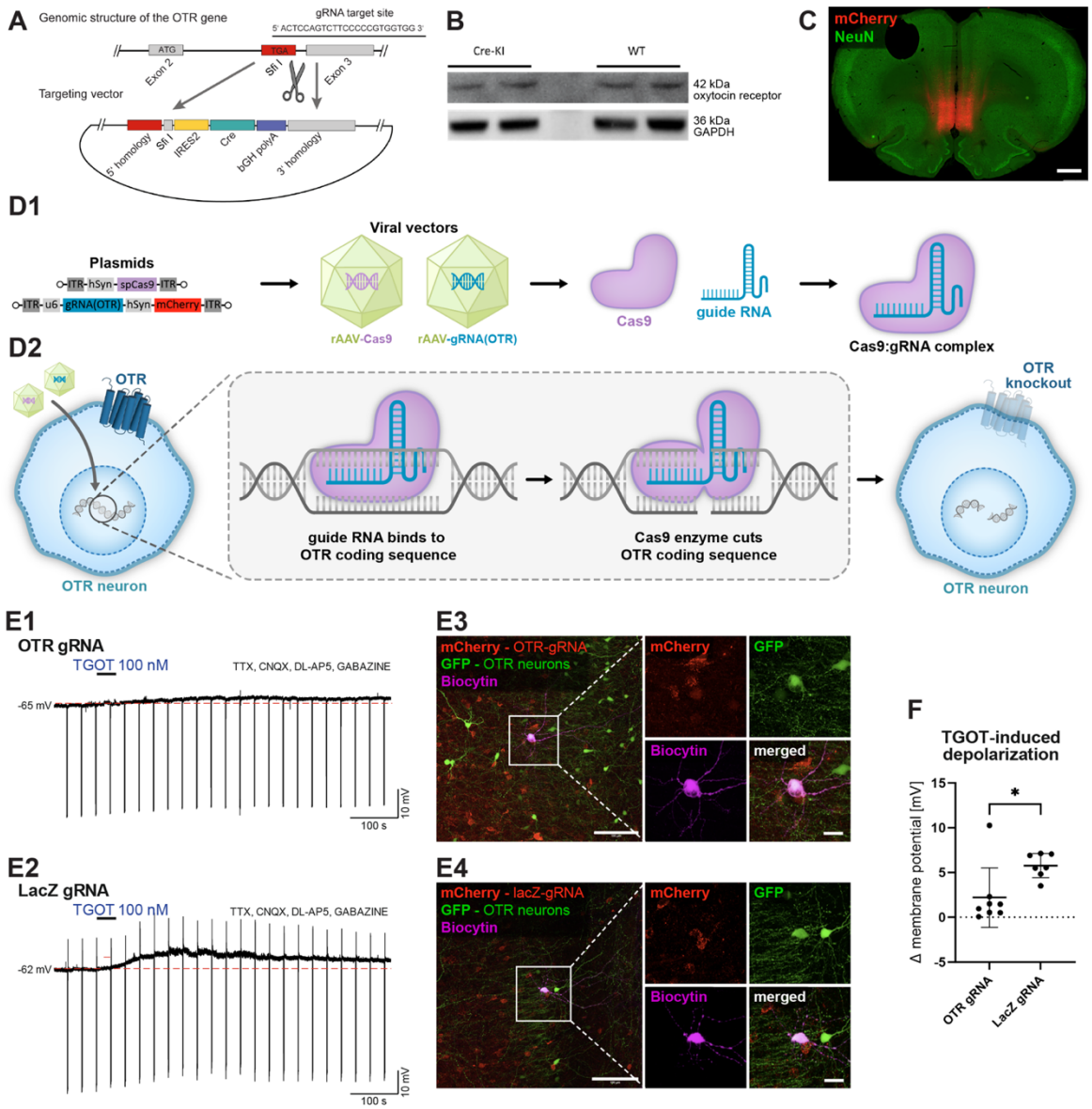

Extended Data Figure 2.

A Generation of the transgenic OTR-Cre rat line utilizing CRISPR/Cas9.

B Western blot analysis of the OTR-levels in both transgenic rat line (Cre-KI) and wildtype (WT).

C Injection site of the Cas9/gRNA virus system injected into the ILC.

D Mechanism of OTR knockout in neurons utilizing a viral CRISPR/Cas9 approach. **D1** Two viral vector plasmids are used to produce rAAVs expressing either the Cas9 enzyme or a specific guide RNA for OTR. **D2** After injection of the mixture of both viruses into the ILC, the Cas9:gRNA complex splices the OTR coding sequence in all neurons and leads to a functional OTR knockout, while the neurons themselves remain viable. As a control, a guide RNA for lacZ is used, as no unspecific splicing is expected.

E Representative traces of a whole-cell patch clamp recordings (current clamp, zero current mode) obtained from an OTR+ ILC neuron transfected with AAVs carrying **E1** Cas9 and OTR gRNA or **E2** Cas9 and LacZ gRNA. A profound TGOT-induced depolarization in the control condition (LacZ) and its absence in the OTR knockout was observed. Downward deflections represent voltage responses of the recorded neuron to hyperpolarizing current injections. **E3** Series of fluorescent projection images of biocytin-filled OTR+ ILC neurons transfected with AAVs carrying Cas9 and OTR gRNA or **E4** Cas9 and LacZ gRNA.

F TGOT-induced depolarization is significantly reduced in the OTR+ ILC neurons transfected with AAVs carrying Cas9 and OTR gRNA compared to the control condition.

Figure S3

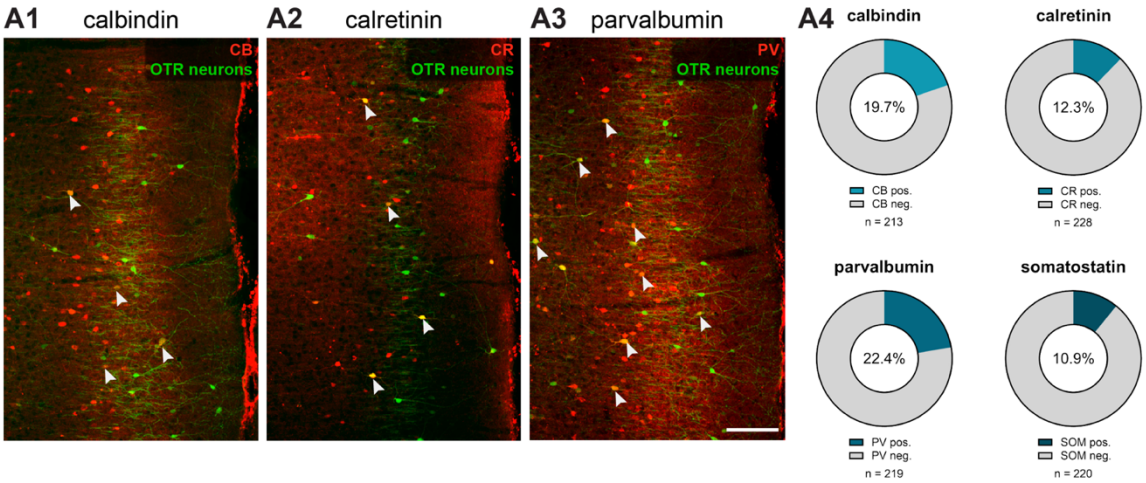

Extended Data Figure 3.

A Heterogenous OTR interneuron population in the ILC. **A1-A3** Representative images of ILC sections previously injected with a Cre-dependent rAAV expressing GFP in OTR neurons and counterstained for various interneuron markers: calbindin (CB), calretinin (CR) and parvalbumin (PV). Scalebar. **A4** Quantitative analysis of the OTR interneuron population; both calbindin or parvalbumin are expressed in about 20% of OTR interneurons in the ILC, while calretinin or somatostatin are found in 10% of interneurons. Scalebar 150µm.

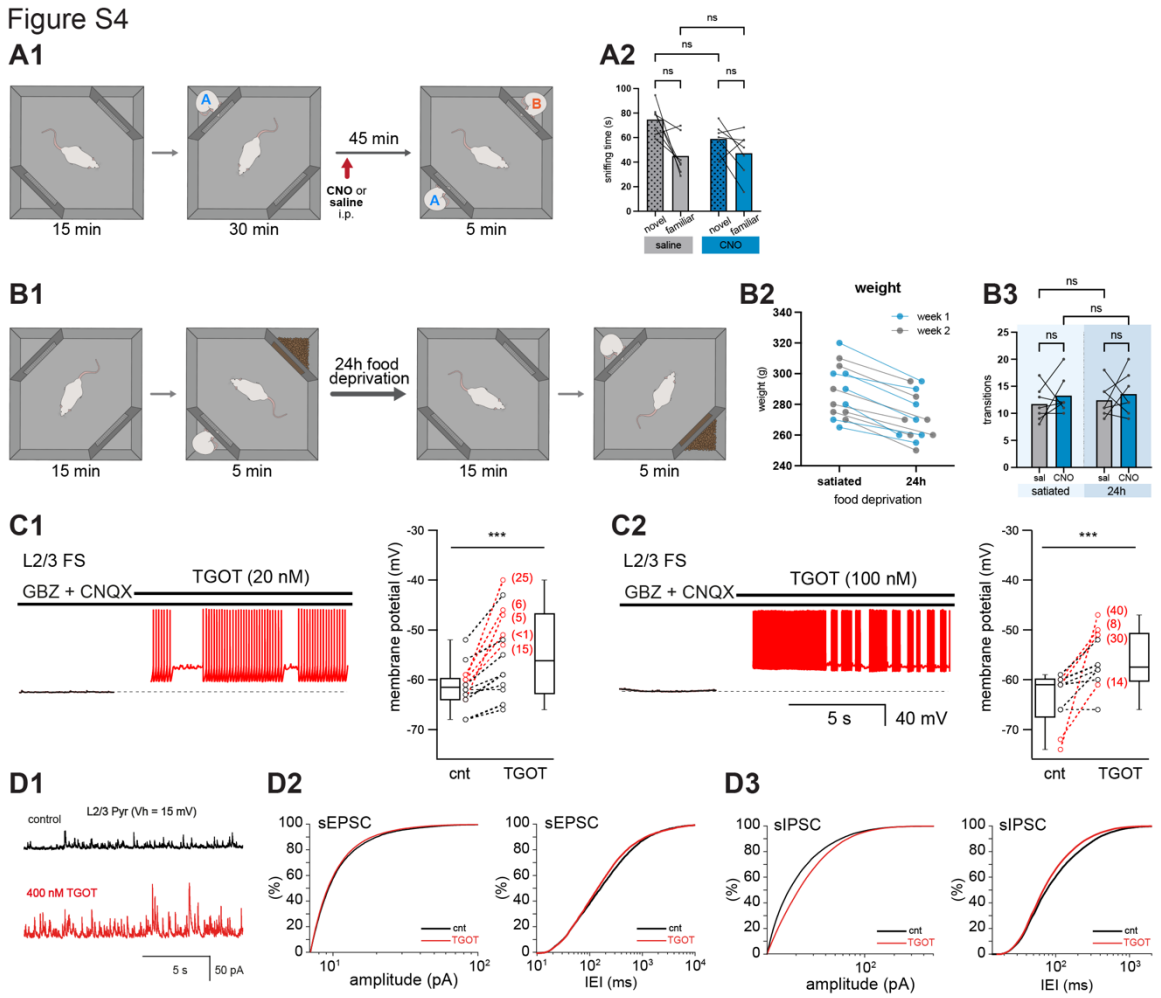

Extended Data Figure 4.

A Social novelty preference paradigm. **A1** Paradigm timeline: animals were habituated to an open field arena with two empty corner compartments for 15 minutes, before placing an unknown female conspecific (animal A) into one corner for a 30 min familiarization session; after a 45 min break, both the familiar (A) and a novel (B) conspecific rat were placed in opposite corners, in order to test social memory. CNO was administered 40 min before the start of the 5 min test session. Corners were placed randomly and altered between sessions and animals. **A2** No effect of CNO administration was observed compared to saline administration (n=7 animals).

B Food vs. social behavior paradigm. **B1** Paradigm timeline: animals were habituated to an open field arena with two empty corner compartments for 15 minutes, before placing an unknown female conspecific into one corner, and food into the opposite corner; after 24h of food deprivation the test was repeated. CNO was always injected 40 min before the start of the 5 min choice session. Corners were placed randomly and altered between sessions and animals. **B2** Weight loss of rats after 24h of food deprivation was verified for both weeks of experiments (due to the within-subject approach, animals were subjected to the paradigm twice for the two conditions (saline vs. CNO, counterbalanced between the two weeks), therefore the two sessions were separated by 6 days of ad libitum access to food to allow the rats to return to their original body weight. **B3** The number of transitions from one corner to the other (food to social or social to food) was unaltered by food deprivation or CNO application (n=7 animals).

C Representative traces of whole-cell patch clamp recordings (current clamp, zero current mode) and quantitative analysis of membrane potential changes in layer 2/3 fast-spiking interneurons upon bath application of either **C1** 20nM TGOT (n=12 cells, brain slices obtained from 5 rats; p<0.001 Wilcoxon Signed Rank test) or **C2** 100nM TGOT (n=10 cells, brain slices obtained from 4 rats; p=0.004 Wilcoxon Signed Rank test).

D Analysis of EPSCs (n=37) and IPSCs (n=38) of layer 2/3 OTR negative pyramids after TGOT application (400nM) compared to baseline (cnt). The brain sections were obtained from 10 rats. **D1** Representative trace of IPSC recording. **D2** No effect on EPSC amplitude or kinetics was observed, however **D3** IPSC amplitude (and charge transferred) are increased (20.7 ± 2.3 vs. 23.6 ± 1.8 pA, p = 0.0017; 2173 ± 222 vs. 2657 ± 837 pC, p=0.0013, respectively). IEI: inter-event-interval.

Figure S5

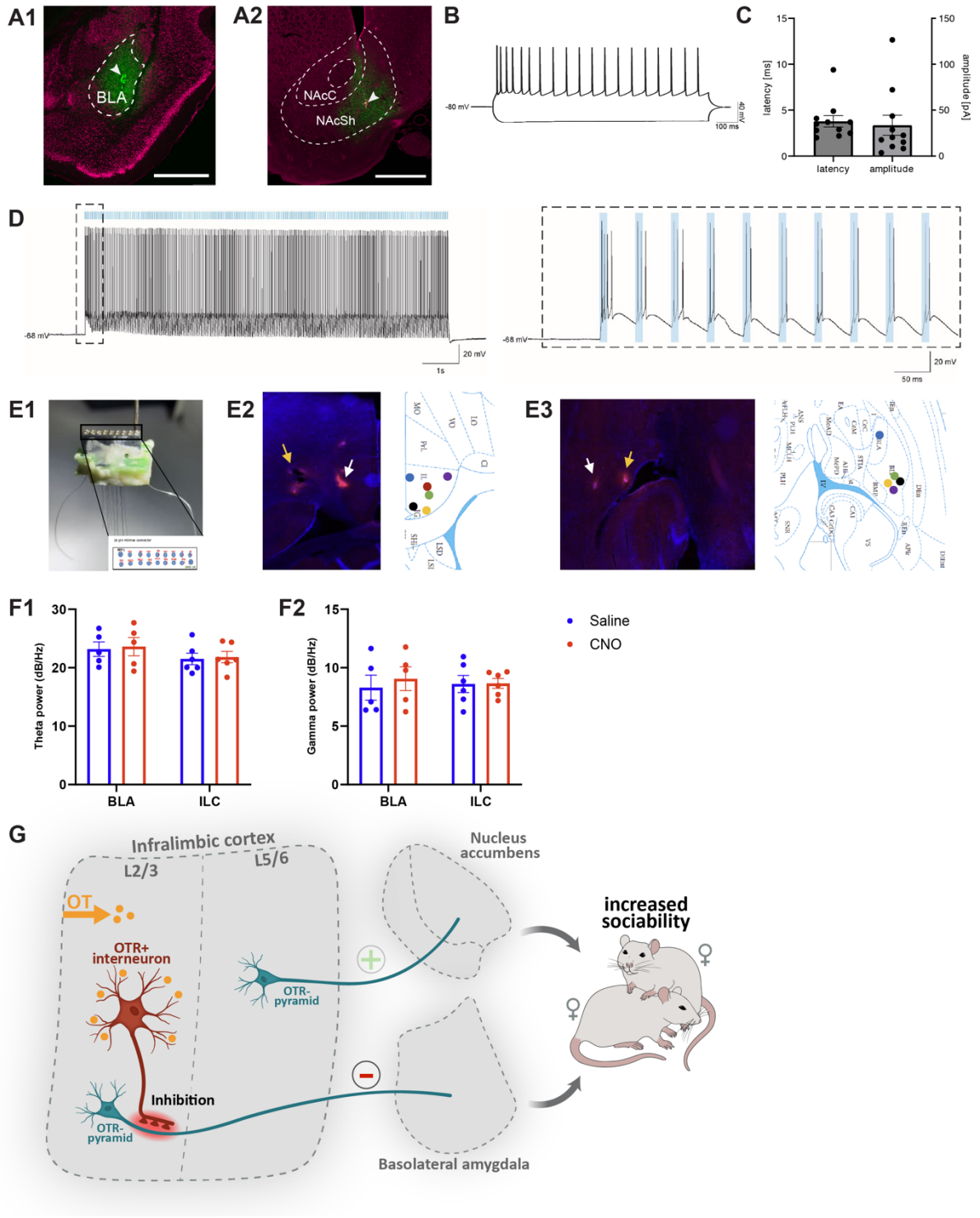

Extended Data Figure 5.

A Representative injection sites of retro-AAV-hSyn-GFP in the **A1** BLA or **A2** NAc. The position of the pipette tip during the injection is marked with retrobeads (white arrow).

B Representative traces of a whole-cell patch clamp recordings (current clamp, zero current mode) obtained from a BLA-projecting ILC neuron showing spike frequency adaptation typical for pyramidal cells.

C Latency and amplitude of BLA-projecting pyramidal neurons (n=11)

D Representative traces of a whole-cell patch clamp recordings (current clamp, zero current mode) obtained from an OTR$^+$ ILC interneuron expressing ChR2 and following to BL stimulation (20Hz, 10ms long pulses, ~10mW). The right trace shows a zoom of the first 10 stimulations.

E *In vivo* electrophysiological recordings of LFPs in ILC and BLA. **E1** A picture of a microelectrode array (MEA) before implantation, with inset showing a scheme of the connector's pins. Note that multiple electrodes are located nearby and may be implanted in the same area. **E2** Left: Horizontal section of the prefrontal cortex (stained blue with DAPI), showing in red the DiI traces left by the electrodes. White arrow indicates the tip location of the on-target electrode used for the analysis of ILC signals, while the yellow arrow indicates tip locations of off-target electrodes. Right: Brain atlas scheme of the horizontal slice shown in E2, with ILC electrode locations from all recorded animals. **E3** Left: Horizontal section of the BLA (marked blue with DAPI), showing the DiI traces in red left by the electrodes. White arrow indicates the tip location of the on-target electrode used for the

analysis of BLA signals, while the yellow arrow indicates tip locations of off-target electrodes. Right: Brain atlas scheme of the horizontal slice shown in E3, depicting BLA electrode locations from all recorded animals.

F1 Mean (±sem) theta power recorded during the 5-min baseline period, before stimuli introduction to the arena, from the BLA (left, n=5 animals) and ILC (right, n=6 animals), 30 min after injection of either saline (blue bars) or CNO (red bars) to the recorded rats. **F2** As in F1, for gamma power.

G Working hypothesis. OT projections from the hypothalamus innervate the infralimbic cortex, where they specifically activate OTR^+ interneurons in layer 2/3. These OTR^+ interneurons, which show functional and anatomical properties of chandelier interneurons, preferentially target and inhibit OTR^- pyramidal neurons projecting to the basolateral amygdala (BLA), decreasing neuronal activity in the BLA. Specific and targeted activation of this OTR^+ neuronal population increases sociability and social preference in female rats.